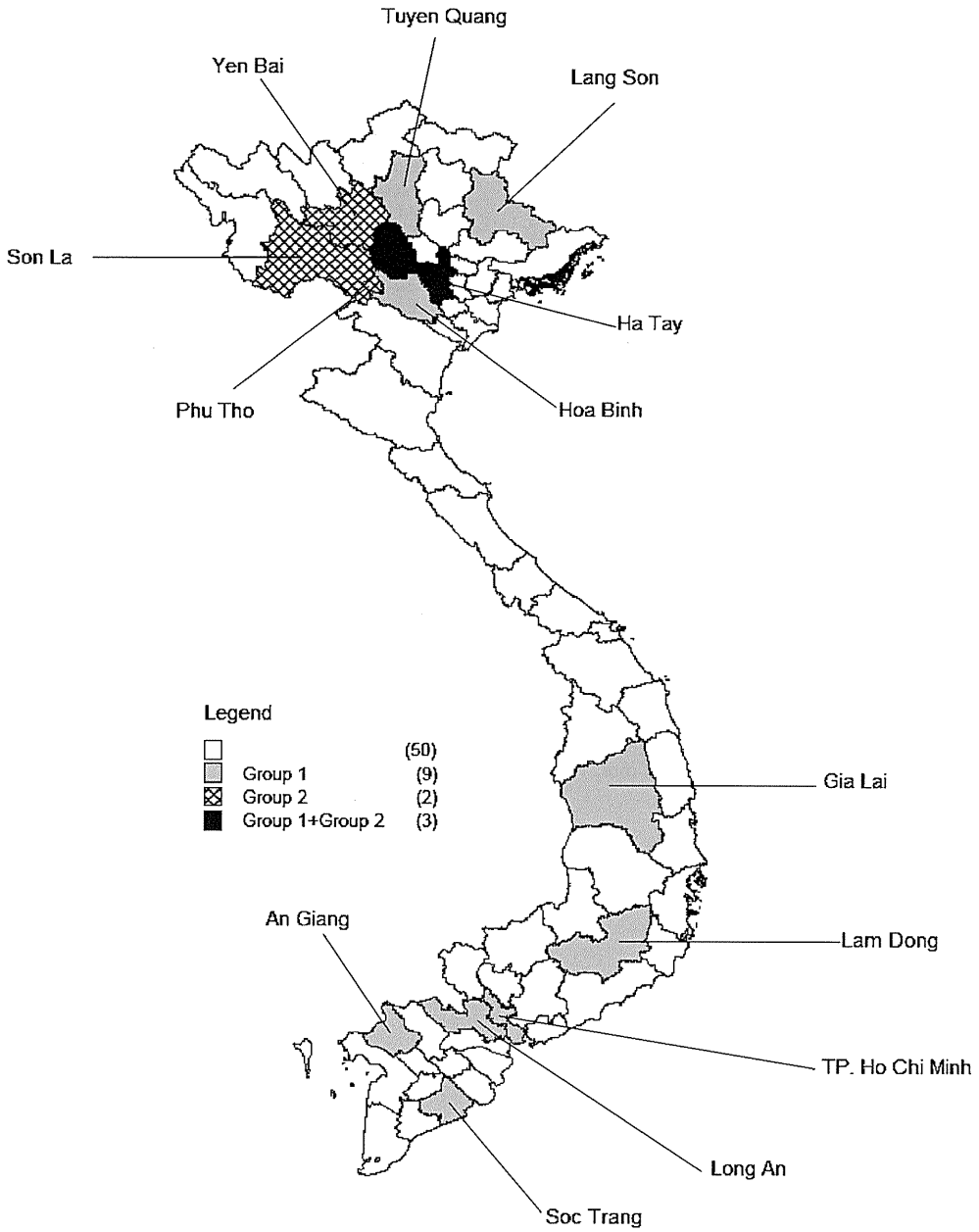

Fig. 2. Topography of RABV strains isolated in Vietnam, 2006–2009. Topographical chart was constructed by HealthMapper software, version 4.2 which is supported by World Health Organization.

be implemented throughout the country. RABV was detected in 2 of the 100 sick dogs (2%) from slaughterhouses located in the northern provinces of Vietnam (Table 1). Previous studies suggest that since some of the infected patients were never bitten by dogs or cats, they must have been infected while butchering the sick dogs or cats (1,3,5,7,15).

The findings of the molecular study showed that at least two different genetic groups of RABV are circulating in Vietnam. Group 1 included strains isolated in Vietnam, and these strains were closely related to those isolated in China, Malaysia, Thailand, and the Philippines. Group 2 consisted of RABVs isolated from humans and dogs in the northern provinces of Vietnam, and these strains were genetically similar to those isolated in southern China (Fig. 1). This finding suggests that the recent increase in cases of infections with Group 2 RABV can be attributable to a constant influx of RABVs from China into Vietnam or vice versa. A previous molecular study conducted by Yamagata et al. (14) in Ho Chi Minh City, Vietnam found that the RABV strains from Vietnam belonged to the South East Asia 1 genotype and were similar to the isolates from Thailand and strain N11 from Guangxi province of China. Further, evidence on the presence of the distinct subgroups in Group 1 (Fig. 1) suggests that RABV may have independently entered Vietnam from several countries such as China, the Philippines, Thailand, and Malaysia and may have established and spread throughout Vietnam.

Strict border control should be implemented to mitigate further influx of RABV from neighboring countries. Although the incidence of rabies due to circulating RABVs in slaughterhouses is less common than

that due to dog bite, the national program for rabies control and prevention in Vietnam should include monitoring of the health of dogs meant for human consumption and vaccination for workers at dog slaughterhouses. Further, monitoring of and research on the circulating RABVs in dog markets may help to determine the cause of rabies and control the spread of rabies in slaughterhouses in Vietnam.

Acknowledgments We would like to thank Dr. Huong Thanh Nguyen (Epidemiology Department, National Institute of Hygiene and Epidemiology, Hanoi, Vietnam) for her help on construction of rabies epidemiology map.

This study was financially supported by the Ministry of Health, Welfare and Labour, Japan and the Ministry of Health, Vietnam.

Conflict of interest None to declare.

REFERENCES

1. Aguilar, E. (2008): Rabies Feared in 30 Dog Meat Eaters. Philippines Daily Inquirer. January 13, 2008.
2. Bounlay Phommasack, et al. (2008): "Country Report on Rabies Control and Prevention in LDR", ASEAN + 3 Conference on Sharing Information on Rabies and Prevention. Halong, Vietnam, April 2008.
3. Wertheim, H.F.L., Nguyen, T.Q., Nguyen, K.A.T., et al. (2009): Furious rabies after an atypical exposure. Plos Med., 6(3), 1-5.
4. Nguyen, H.T. (2009): Rabies in Vietnam. 2nd International Rabies in Asia Conference (RIACON) Proceeding. Hanoi, Vietnam, September 2009.
5. Childs, J.E. (2002): Rabies. Routes of Rabies Virus Transmission to Humans. p. 125-126. Academic Press.
6. Knobel, D., L., Cleaveland, S., Coleman, P.G, et al. (2005): Re-evaluating the burden of rabies in Africa and Asia. Bull. World Health Organ., 83, 1-11.
7. Kureishi, A., Xu, L.Z., Wu, H., et al. (1992): Rabies in China: recommendations for control. Bull. World Health Organ., 70, 443-475.
8. Van, K.D. (2008): "Animals Rabies Control and Prevention in Vietnam", ASEAN + 3 Conference on Sharing Information on Rabies and Prevention. Halong, Vietnam, April 2008.
9. Larkin, M.A., Blackshields, G., Brown, N.P., et al. (2007): Clustal W and Clustal X version 2.0. Bioinformatics, 23, 2947-2948.
10. Deray, R.A. (2008): "Human Rabies in the Philippines", ASEAN + 3 Conference on Sharing Information on Rabies and Prevention. Halong, Vietnam, April 2008.
11. Heng, S. (2008): "Rabies Situation in Cambodia", ASEAN + 3 Conference on Sharing Information on Rabies and Prevention. Halong, Vietnam, April 2008.
12. Tamura, K., Dudley, J., Nei, M. et al. (2007): MEGA4: Molecular Evolutionary Genetics Analysis (MEGA) software version 4.0. Mol. Biol. Evol., 24, 1596-1599.
13. Zhen, X. (2008): "Situation, Surveillance and Control of Rabies in Mainland, China", ASEAN + 3 Conference on Sharing Information on Rabies and Prevention. Halong, Vietnam, April 2008.
14. Yamagata, J., Ahmed, K., Khawplod, P., et al. (2007): Molecular of rabies in Vietnam. Microbiol. Immunol., 51, 833-840.
15. Wallerstein, C. (1999): Rabies cases increase in the Philippines. Br. Med. J., 318, 1306.

Jpn. J. Infect. Dis., 64, 463-472, 2011

Original Article

Gene Expression Analysis of Host Innate Immune Responses in the Central Nervous System following Lethal CVS-11 Infection in Mice

Naoko Sugiura[1,3], Akihiko Uda[1], Satoshi Inoue[1,3]*, Daisuke Kojima[2], Noriko Hamamoto[1,3], Yoshihiro Kaku[1], Akiko Okutani[1], Akira Noguchi[1], Chun-Ho Park[2], and Akio Yamada[1,3]

[1]*Department of Veterinary Science, National Institute of Infectious Diseases, Tokyo 162-8640;*
[2]*Department of Veterinary Pathology, School of Veterinary Medicine, Kitasato University, Aomori 034-8628; and*
[3]*United Graduate School of Veterinary Science, Gifu University, Gifu 501-1193, Japan*

(Received August 12, 2011. Accepted September 9, 2011)

SUMMARY: The central nervous system (CNS) tissue of mice infected with the CVS-11 strain of rabies virus (RABV) was subjected to gene expression analysis using microarray and canonical pathway analyses. Genes associated with innate immunity as well as inflammatory responses were significantly up-regulated, corroborating with the previous findings obtained using attenuated viruses that did not induce a fatal outcome in infected mice. Histopathological examination showed that neurons in the cerebellum had undergone apoptosis. Although the extent of Fas ligand up-regulation was not so prominent, perforin and granzyme genes were highly expressed in the CNS of mice infected with CVS-11. The presence of perforin and granzymes both in the Purkinje cells and CD3 T lymphocytes strongly suggested that apoptosis of the former cells was induced by the latter cells.

INTRODUCTION

Rabies virus (RABV), a member of the genus *Lyssavirus* of the family *Rhabdoviridae*, is known to cause fatal encephalomyelitis in many mammalian species (1). Annually, more than 55,000 individuals die of rabies worldwide. There is often little or no histopathological evidence of neural destruction in animals dying of rabies (2), and the functional changes in RABV infected neurons in vitro are minimal (3). The mechanism underlying RABV infection induced fatal clinical disease and the pathogenesis of rabies are not completely understood.

The neurovirulence of RABV has been mainly studied using animal models that were infected with laboratory strains (fixed virus) having different degrees of pathogenicity. Infection of animals with highly attenuated strains of RABV is not lethal, and profound inflammation accompanied by apoptosis and neural degeneration in the central nervous system (CNS) is noted in such animals. The induction of innate immune responses in the CNS is a hallmark of infection with highly attenuated strains, whereas neural damage is absent or minimal and innate immune responses are not induced in animals infected with street (wild) strains of RABV. A recent study suggested that up-regulation of genes encoding interferon alpha/beta (IFN-α/β) signaling pathways and chemokines was responsible for the elimination of highly attenuated strains from the CNS of infected animals.

Although the challenge virus standard (CVS) strains are a type of fixed RABV, there are several strains of CVS that differ in pathogenicity in different animals. The CVS-24 and CVS-11 have neuroinvasive characteristics and can invade the spinal cord and brain following peripheral inoculation, resulting the death of the infected animals with paralytic symptoms (4–6). In contrast, the CVS-B2c strain, a cloned version of CVS-24, was less pathogenic in adult mice when inoculated intramuscularly. The CVS-F3 strain is apathogenic even in immunocompetent adult mice regardless of the route of infection and causes a transient weight loss in normal mice (7–9).

To precisely understand the mechanisms underlying the pathogenicity of RABV infection, it is crucial to use animal models that most closely reproduce the natural infection. However, conflicting results, in terms of the activation of inflammatory host responses or apoptosis, were sometimes noted even though the same virus strain (CVS-11) was used in these experiments. We hypothesized that these differences were likely caused by a subtle difference in the pathogenicity of respective virus strains used in the experiments.

The aim of this study is to obtain gene expression profiling data from mice infected with pathogenic CVS-11 strain and compare these data with those reported previously in the literature. Although directly comparing the data obtained in different studies is difficult, careful comparison of the data might enable understanding of the possible roles of particular genes involved in the progression of rabies. We expected to elucidate the reason for the conflicting results reported by different studies.

MATERIALS AND METHODS

Cells and virus: Mouse neuroblastoma (MNA) cells were cultivated in minimum essential medium Eagle

*Corresponding author: Mailing address: Department of Veterinary Science, National Institute of Infectious Diseases, 1-23-1 Toyama, Shinjuku-ku, Tokyo 162-8640, Japan. Tel: +81-3-5285-1111, Fax: +81-3-5285-1179, E-mail: sinoue@nih.go.jp

(MEM) (Sigma, St. Louis, Mo., USA) supplemented with 10% heat-inactivated fetal bovine serum (FBS) (Sigma), penicillin (100 U/ml), and streptomycin (100 μg/ml) (Gibco, Invitrogen, Carlsbad, Calif., USA) (MEM-10% FBS). The CVS-11 strain of RABV and MNA cells were kindly provided by Dr. C. E. Rupprecht (Poxvirus and Rabies Branch, DHCPP, NCEZID, CDCP, Atlanta, Ga., USA). The CVS-11 strain was propagated in the MNA cells as described previously (10) and stored at −80°C until use.

Infection of mice with RABV: Six-week-old female C57BL/6J mice were purchased from SLC, Inc., Shizuoka, Japan. Virus suspension (100 μl) containing 10^7 focus-forming units (FFU) of CVS-11 were intramuscularly inoculated into the left hind limb of 18 mice. Twelve mice were inoculated with MEM in a similar way. Mice were humanely sacrificed under anesthesia on days 3 and 7 post-inoculation (pi), and the brains and spinal cords were removed, snap frozen, and kept at −80°C. All experiments involving laboratory animals were approved by the institutional animal care and use committee (IACUC) and performed according to the guidelines issued by the IACUC.

Virus titration: Virus titration was performed in quadruplicate, as previously reported (11). In brief, 10-fold dilutions of 10% homogenates of the brains and spinal cords prepared in phosphate buffered saline (PBS(−)) were inoculated onto MNA cells grown in 96-well-plates. After 48 h incubation at 35°C, the cells were washed 3 times with PBS(−) and fixed with 80% acetone for 30 min at room temperature (RT). Next, the infected MNA cells were stained with the fluorescein isothiocyanate (FITC)-conjugated anti-RABV nucleoprotein (N) monoclonal antibody (Fujirebio Diagnostics, Inc., Malvern, Pa., USA) diluted 1:100 in PBS(−) with 0.002% Evans blue for 30 min at RT. The cells were washed 3 times with PBS(−), and the screening for the viral antigen was performed using a UV microscope (Eclipse TE200; Nikon, Tokyo, Japan).

Microarray analysis: Total RNA (300 ng) purified from the brain and spinal cord using RNeasy mini kit (Qiagen, Hilden, Germany) was converted into cDNA using a T7-oligo dT primer. Complementary RNA was transcribed using T7 polymerase in the presence of cyanine-3 (Cy3). Following fragmentation, Cy3-labeled cRNA was hybridized to the Whole Mouse Genome Microarray (44 k probes × 4 arrays/slide) (Agilent, Palo Alto, Calif., USA) at 65°C for 16 h in a rotating hybridization oven at a speed of 10 rounds per min (RPM). Microarray slides were washed sequentially with wash solution 1 (Agilent), wash solution 2 (Agilent), and acetonitrile (Wako, Osaka, Japan). Slides were scanned on an Agilent microarray scanner (Agilent), and the image files were analyzed using feature extraction software (Agilent). Data mining was performed using GeneSpring GX 11 (Agilent). The expression data were normalized with per chip normalization (to the 75th percentile) and per gene normalization (baseline to mean of mock samples). The normalized data were filtered by flags (present or marginal) and fold changes (>2.0). Significant changes in gene expression were found using *t* test ($P < 0.05$, Benjamini-Hochberg false discovery rate [FDR]). The filtered genes identified by GeneSpring were subjected to further analysis of protein-protein interactions within the context of signaling pathways by Ingenuity Pathway Analysis (IPA) (Ingenuity Systems, Redwood City, Calif., USA).

Quantification of cytokines and chemokines: The levels of cytokines and chemokines were determined by the fluorescent bead immunoassay by Mouse Th1/Th2 10plex FlowCytomix Multiplex (Bender MedSystem, Vienna, Austria) and Mouse Chemokine 6plex FlowCytomix Multiplex kits (Bender MedSystem), according to manufacturer's instructions. Briefly, clarified homogenates prepared from the brains and spinal cords were mixed with beads conjugated with appropriate antibodies, followed by incubation with biotin-conjugated second antibodies and then with phycoerythrin-labeled streptavidin. Washed beads were resuspended in the assay buffer and subjected to flow cytometry on COULTER Epics XL (Beckman Coulter, Fullerton, Calif., USA). BMS FlowCytomix Pro 2.2 software (Bender MedSystem) was used for calculatig the levels of cytokines and chemokines. IFN-β was measured by Mouse IFN-Beta ELISA (PBL Biomedical Laboratories, Piscataway, N.J., USA).

Immunohistochemistry and TUNEL assay: Distribution of RABV antigens as well as the surface markers for neurons and other cellular components in the CNS was determined by immunohistochemistry (IHC) using paraffin-embedded sections, according to the methods reported by Kojima et al. (12). Polyclonal antibody against the phosphoprotein (anti-P antibody) of RABV was obtained by immunization of a rabbit. Anti-glial fibrillary acidic protein (GFAP) (Nichirei Biosciences, Tokyo, Japan), anti-ionized calcium binding adaptor molecule 1 (Iba1) (Wako), anti-CD3 (DAKO, Kyoto, Japan), and anti-CD20 (Spring Bioscience, Fremont, Calif., USA) were used to identify astroglia, microglia, T lymphocytes, and B lymphocytes, respectively. Perforin and granzymes were detected using a rat monoclonal antibody to perforin (Abcam, Cambridge, UK) and biotinylated anti-mouse granzyme B antibody (R&D Systems, Inc, Minneapolis, Minn., USA), respectively. The TUNEL assay was performed as previously described (12,13).

RESULTS

Clinical signs and viral loads: C57BL/6J mice inoculated with CVS-11 showed severe hind limb paralysis on day 7 pi. Of the 9 mice, 4 showed severe paralysis in only 1 hind limb to which the virus was inoculated, whereas the remaining 4 mice showed paralysis of both the hind limbs. Quadriplegia was apparent in 1 mouse. Virus titers in the brains were 1.8 × 10 FFU/mg on day 3 pi and 2.3 × 10^5 FFU/mg on day 7 pi, and those in the spinal cords were 6.5 × 10 FFU/mg on day 3 pi and 5.7 × 10^3 FFU/mg on day 7 pi.

Microarray analysis: No significant change (fold change >2.0, $P < 0.05$) in the expression level of 41,252 genes in the brains and spinal cords was noted in the mice 3 days after infection with the CVS-11 strain. However, after 7 days of infection, significant changes in gene expression levels were noted in the brains and spinal cords of the infected mice. The results are summarized in a Venn diagram (Fig. 1) by GeneSpring GX 11. Brain specific changes were recognized in the expres-

sion profiles of 1,674 genes, and 1,436 of 1,674 genes were mapped by IPA software using Ingenuity Knowledge Base. Of the 1,436 genes, 780 were up-regulated and 656 were down-regulated by the infection. In the spinal cord, 2,101 genes that showed differential expression were mapped and, of these 640 genes were up-regulated. Interestingly, genes associated with innate immune responses were commonly up-regulated in both the brain and spinal cord (Table 1). Normalization of the data did not affect this propensity, in that, the genes related to innate immune responses, especially those associated with inflammation, such as chemokines, IFNs, and IFN-related genes, were remarkably up-regulated (Table 2). The expression level of IFN-α/β genes was remarkably higher in the brains than in the spinal cords. The gene expression of IFN-β1 and IFN-γ was markedly up-regulated both in the brain and in spinal cord (fold change, 156.5 to 772.3). The levels of genes associated with the activation of IFN signaling pathways were moderately elevated compared to those of IFN-α/β genes. Most genes encoding chemokines were considerably up-regulated. Interleukin (IL) genes and IL-related genes were also up-regulated but to a lesser extent compared to genes encoding chemokines. IL-6 was the only gene that showed high expression level comparable to that of chemokine genes. The expression of CD3 and CD8 genes in the brains and spinal cords showed slight elevation after RABV infection. Expression of genes associated with the elimination of cytotoxic T lymphocytes (CTLs), particularly granzyme genes, was up-regu-

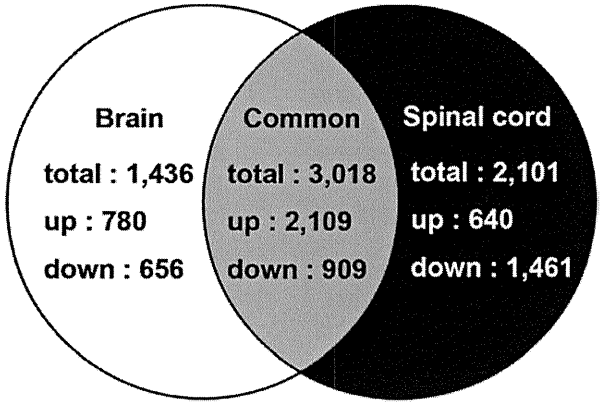

Fig. 1. Venn diagram of up- or down-regulated genes in the brains and the spinal cords after CVS-11 infection. Mice intramuscularly inoculated with 10^7 FFU of CVS-11 into the left hind limb were humanely euthanized on day 7 pi. Mock-infected mice were also sacrificed as controls. RNA ($n = 6$) extracted from the brains and the spinal cords were converted to cDNAs and were subjected to the microarray analysis using Agilent Microarray, feature extraction software and GeneSpring software. The normalized data were filtered by flag and >2-fold changes ($P < 0.05$).

Table 1. Top 10 of biological function categories by IPA

Category	Function Annotation	*P*-value
Common	immune response	6.41E-82
	developmental process of leukocytes	2.20E-62
	developmental process of mononuclear leukocytes	1.38E-58
	developmental process of blood cells	2.23E-58
	activation of leukocytes	4.46E-56
	developmental process of lymphocytes	1.34E-53
	development of leukocytes	7.32E-53
	proliferation of blood cells	1.16E-52
	activation of blood cells	1.66E-52
	quantity of leukocytes	2.46E-52
Brain specific	tumorigenesis	3.30E-11
	cancer	7.19E-09
	tumor	1.19E-08
	neoplasia	1.34E-08
	movement of cells	2.21E-08
	migration of cells	3.05E-08
	migration of eukaryotic cells	1.58E-07
	movement of eukaryotic cells	1.74E-07
	inflammatory disorder	6.13E-07
	cell movement	6.80E-07
Spinal cord specific	coronary artery disease	1.29E-08
	arteriosclerosis	2.77E-08
	atherosclerosis	6.44E-08
	cardiovascular disorder	3.41E-07
	vesicoureteral reflux	5.10E-07
	Dupuytren contracture	1.55E-05
	transport of cation	2.52E-05
	organization of collagen fibrils	2.67E-05
	transport of inorganic cation	6.19E-05
	burn	7.22E-05

Table 2. Expression profile of immunoresponse genes in brains and spinal cords

Gene symbol	Annotation	Probe name	Fold chanage over control	
			Brain	Spinal cord
Interferon				
Ifna1	interferon alpha 1	A_51_P436401	44.0	<2.0
Ifna2	Mouse alpha-interferon (MuIFN-alpha)	A_52_P482280	434.7	13.6
Ifna4	interferon alpha 4	A_51_P355829	323.0	12.7
Ifnb1	interferon beta 1	A_51_P144180	772.3	156.5
Ifng	interferon gamma	A_51_P220976	570.5	525.4
Ifng	interferon gamma	A_52_P68893	517.0	408.6
Ifnar2	interferon (alpha and beta) receptor 2	A_52_P190405	2.6	2.6
Interferon response genes				
Stat1	signal transducer and activator of transcription 1	A_52_P496503	14.3	10.3
Stat1	signal transducer and activator of transcription 1	A_52_P70255	28.6	21.7
Stat1	signal transducer and activator of transcription 1	A_52_P505218	16.8	10.9
Stat1	signal transducer and activator of transcription 1	A_52_P70261	32.2	24.7
Stat2	signal transducer and activator of transcription 2	A_51_P225808	7.1	11.6
Stat3	signal transducer and activator of transcription 3	A_51_P201480	4.9	3.4
Stat3	signal transducer and activator of transcription 3	A_52_P569499	3.1	2.8
Irf1	interferon regulatory factor 1	A_52_P175685	44.3	24.8
Irf1	interferon regulatory factor 1	A_51_P146103	54.8	29.4
Irf2	interferon regulatory factor 2	A_51_P316523	4.4	3.4
Irf5	interferon regulatory factor 5	A_51_P346668	20.4	11.7
Irf7	interferon regulatory factor 7	A_51_P421876	189.5	142.1
Irf8	interferon regulatory factor 8	A_52_P354823	22.2	8.2
Irf8	interferon regulatory factor 8	A_51_P187253	18.8	8.5
Jak2	Janus kinase 2	A_51_P483231	4.1	2.9
Jak2	Janus kinase 2	A_52_P309376	2.4	2.4
Oas1a	2′-5′ oligoadenylate synthetase 1A	A_52_P337357	130.5	69.4
Oas1b	2′-5′ oligoadenylate synthetase 1B	A_52_P110877	91.8	43.1
Oas1c	2′-5′ oligoadenylate synthetase 1C	A_51_P428529	6.1	3.6
Oas1e	2′-5′ oligoadenylate synthetase 1E	A_51_P134030	4.9	3.5
Oas1f	2′-5′ oligoadenylate synthetase 1F	A_51_P154842	125.2	62.0
Oas1g	2′-5′ oligoadenylate synthetase 1G	A_51_P355267	13.2	13.0
Ifi35	interferon-induced protein 35	A_51_P414889	39.0	24.5
Ifit1	interferon-induced protein with tetratricopeptide repeats 1	A_51_P327751	115.4	72.0
Ifit3	interferon-induced protein with tetratricopeptide repeats 3	A_51_P359570	76.4	85.4
Ifitm1	interferon induced transmembrane protein 1	A_52_P541802	6.5	2.9
Psmb8	proteosome (prosome, macropain) subunit, beta type 8 (large multifunctional peptidase 7)	A_51_P345367	104.4	48.7
Psmb8	proteosome (prosome, macropain) subunit, beta type 8 (large multifunctional peptidase 7)	A_51_P345366	101.9	40.4
Tap1	transporter 1, ATP-binding cassette, sub-family B (MDR/TAP)	A_51_P100327	116.6	63.3
Mx1	myxovirus (influenza virus) resistance 1	A_52_P446431	444.5	268.3
Mx1	myxovirus (influenza virus) resistance 1	A_52_P614259	383.7	235.5
Mx2	myxovirus (influenza virus) resistance 2	A_51_P514085	111.4	47.9
H2-Aa	histocompatibility 2, class II antigen A, alpha	A_52_P343306	1.5	14.5
H2-Ab1	histocompatibility 2, class II antigen A, beta 1	A_51_P215237	1.4	12.4
H2-Ab1	histocompatibility 2, class II antigen A, beta 1	A_52_P570717	1.2	10.3
H2-Ab1	histocompatibility 2, class II antigen A, beta 1	A_51_P215242	1.4	12.9
Chemokine				
Ccl2	chemokine (C-C motif) ligand 2	A_51_P286737	595.4	352.8
Ccl3	chemokine (C-C motif) ligand 3	A_51_P140710	158.8	82.8
Ccl4	chemokine (C-C motif) ligand 4	A_51_P509573	205.7	98.5
Ccl5	chemokine (C-C motif) ligand 5	A_52_P638459	344.1	183.2
Ccl5	chemokine (C-C motif) ligand 5	A_51_P485312	433.5	213.1
Ccl7	chemokine (C-C motif) ligand 7	A_52_P208763	146.4	193.8
Ccl7	chemokine (C-C motif) ligand 7	A_51_P436652	221.2	241.7
Ccl8	chemokine (C-C motif) ligand 8	A_51_P464703	102.1	68.9
Ccl12	chemokine (C-C motif) ligand 12	A_52_P249514	104.5	71.8
Cxcl9	chemokine (C-X-C motif) ligand 9	A_51_P461665	1072.3	289.2
Cxcl10	chemokine (C-X-C motif) ligand 10	A_51_P432641	688.3	358.5

Continued on following page

Table 2—Continued

Gene symbol	Annotation	Probe name	Fold change over control	
			Brain	Spinal cord
Cxcl11	chemokine (C-X-C motif) ligand 11	A_52_P676403	410.2	68.7
Cxcl13	chemokine (C-X-C motif) ligand 13	A_51_P378789	209.8	192.3
Interleukin				
Il1a	interleukin 1 alpha	A_52_P100926	8.4	4.0
Il1a	interleukin 1 alpha	A_51_P438283	6.1	3.2
Il1b	interleukin 1 beta	A_51_P212782	32.9	2.3
Il6	interleukin 6	A_51_P217218	357.2	75.0
Il10	interleukin 10	A_51_P430766	13.5	14.3
Il12b	interleukin 12b	A_51_P385812	59.1	31.4
Tnf	tumor necrosis factor	A_51_P385099	83.4	23.2
IL15 related genes				
Il2ra	interleukin 2 receptor, alpha chain	A_52_P277016	8.5	8.3
Il2ra	interleukin 2 receptor	A_51_P118945	6.9	4.0
Il2rb	interleukin 2 receptor, beta chain	A_51_P286496	29.9	25.2
Il2rg	interleukin 2 receptor, gamma chain	A_51_P456952	22.8	14.1
Il15	interleukin 15	A_52_P15461	5.1	3.8
Il15ra	interleukin 15 receptor, alpha chain	A_51_P202292	6.0	4.2
Il15ra	interleukin 15 receptor, alpha chain	A_52_P55902	5.1	3.5
Cellular activation/Differentiation				
Cd3d	CD3 antigen, delta polypeptide	A_51_P285206	21.2	19.2
Cd3g	CD3 antigen, gamma polypeptide	A_51_P260889	11.6	11.0
Cd8a	CD8 antigen, alpha chain	A_52_P443334	16.8	8.7
Cd8a	CD8 antigen, alpha chain	A_51_P345121	40.4	19.6
Cd8b1	Mouse T-cell membrane glycoprotein (Ly-3)	A_51_P150433	46.2	14.0
Apoptosis related genes				
Casp1	caspase 1	A_51_P142861	11.9	13.0
Casp4	caspase 4	A_51_P511787	112.5	33.6
Casp7	caspase 7	A_51_P414548	6.4	4.2
Casp7	caspase 7	A_52_P260114	7.6	4.4
Casp8	caspase 8	A_51_P247799	11.4	7.5
Fas	Fas (TNF receptor superfamily member)	A_51_P345393	7.4	3.7
Fasl	Fas ligand (TNF superfamily, member 6)	A_52_P77106	14.2	15.2
Fasl	Fas ligand (TNF superfamily, member 6)	A_52_P173985	3.7	5.1
Prf1	perforin 1 (pore forming protein)	A_52_P335178	58.1	61.0
Gzma	granzyme A	A_51_P162794	192.4	96.1
Gzmb	granzyme B	A_51_P333274	546.1	389.6

lated. Canonical pathway analysis indicated that IFN signaling pathway (Fig. 2A) as well as the IL-15 production and signaling pathways was activated (Fig. 2B, 2C). Granzyme B signaling pathway and perforin pathway were also activated in the brains and spinal cords of infected mice (Fig. 2D).

Detection of cytokines: Microarray analysis revealed that RABV infection activated the genes associated with innate immune responses. We, therefore, attempted to determine whether the corresponding proteins were expressed in the brains and spinal cords of infected animals. As shown in Fig. 3A, CCL2, CCL3, CCL5, and CCL7 were highly overexpressed in the brains and spinal cords of infected animals, while CCL4 was expressed only in the brains. The expression of IFN-β and IFN-γ in the brains and spinal cords of infected mice was higher than that in uninfected mice (Fig. 3B). Among the ILs investigated, IL-6 was significantly expressed in the RABV-infected animals. There was a low but significant increase in the production of tumor necrosis factor-alpha (TNF-α), while there was hardly any changes in the expression of other ILs after infection with RABV (Fig. 3C).

Immunohistochemical analysis: Next, we focused on the difference in the expression of some antigens in the infected brains and spinal cords, as revealed by immunohistochemical staining. RABV antigens were hardly detected in the neural cells of the brains and spinal cords 3 days after infection; however, on day 7 pi, viral antigens were widely distributed in the cerebellum as well as in the spinal cords (Fig. 4A). No RABV antigens were detected in mock mice. CD3-positive T lymphocytes and Iba1-positive microglia/macrophages were found in not only the cerebellum but also the spinal cords (Fig. 4B and 4C). However, CD-20-positive B lymphocytes could not be detected. As shown in Fig. 4D, apoptotic neural cells (Purkinje cells) were observed. These Purkinje cells contained cytoplasmic RABV antigens that were detected using anti-P antibody. TUNEL assay also revealed that most T lymphocytes were apoptotic. Cells stained for perforin were detected and scattered in the cerebellar peduncle (Fig.

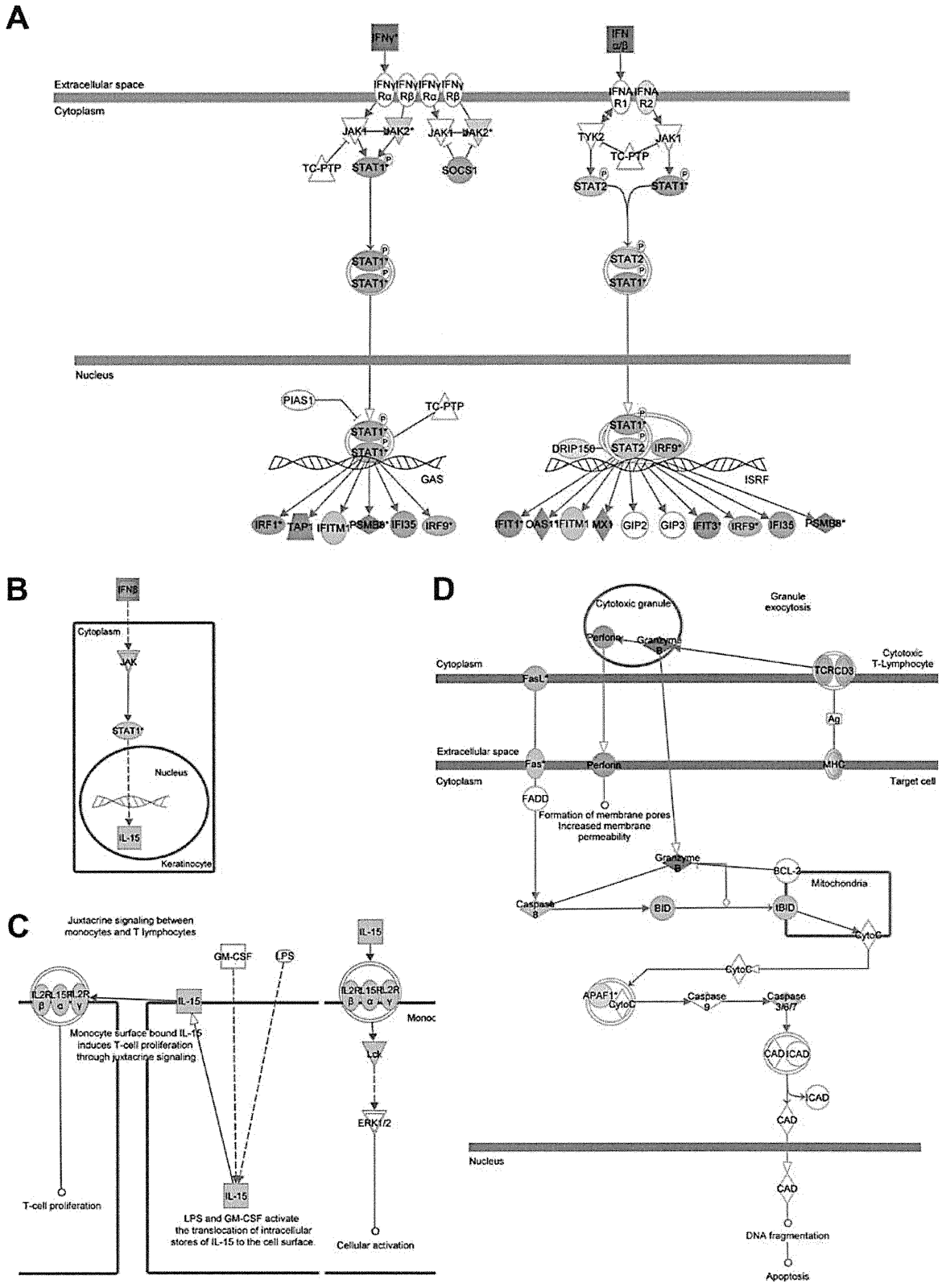

Fig. 2. Pathway analysis of inflammatory responses caused by CVS-11 infection. The genes identified by transcriptome analysis were subjected to Ingenuity Pathway Analysis (IPA). Diagrams show the pathways of interferon signaling (A), IL-15 production (B), IL-15 signaling (C), and Granzyme B signaling (D).

4E) and spinal cords (Fig. 4F). At least 2 cell types, lymphocyte and Purkinje cells, were positive for perforin both in the cerebellum and spinal cords. Granzymes were detected in the Purkinje cells (Fig. 4G) as well as in the infiltrating cells in the spinal cords (Fig. 4H). There was no prominent infiltration of CD3-positive T lymphocytes, increase in Iba1-positive microglia/macrophages, TUNEL-positive neural cells, and cells positive for perforin and granzyme in mock mice.

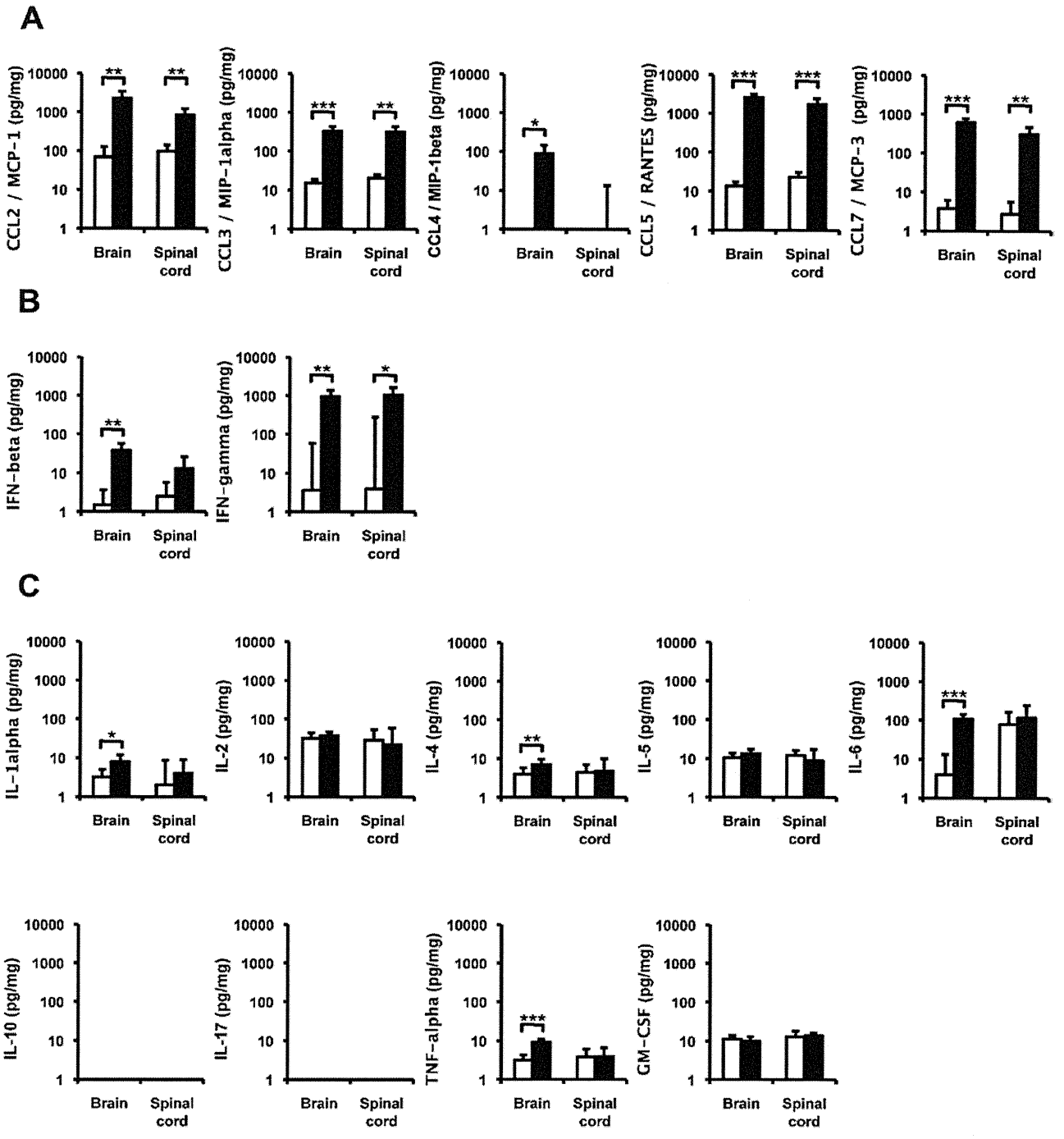

Fig. 3. Production of chemokines and cytokines in the brains and the spinal cords of mice infected with the CVS-11. The brains (n = 6) and the spinal cords (n = 6) were processed as described in the Materials and Methods. Chemokines (A), interferons (B), and cytokines (C) were quantified using the fluorescent bead immunoassay. Statistical significance was determined by Student's t test ($^{*}P < 0.05$, $^{**}P < 0.01$, $^{***}P < 0.001$). The white and black bar indicated mock and infection, respectively.

DISCUSSION

Postmortem examination of the CNS of human rabies victims revealed virtually no histological changes in the neurons (2). Moreover, no inflammatory responses were induced in the CNS of humans who died because of RABV infection (14,15). When laboratory animals were infected with street RABV strains such as silver-haired bat RABV, the pathologic characteristics of RABV infection in humans could be reproduced, in that neither histological changes of infected neurons nor inflammatory responses in the CNS were observed. Animals infected with street viruses, therefore, serve as relevant animal models for better understanding the pathogenesis of rabies. However, extremely high mortality posed by the infection makes it difficult to deal with the street viruses in most laboratories. CVS strain is one of the fixed viruses that retains the ability to in-

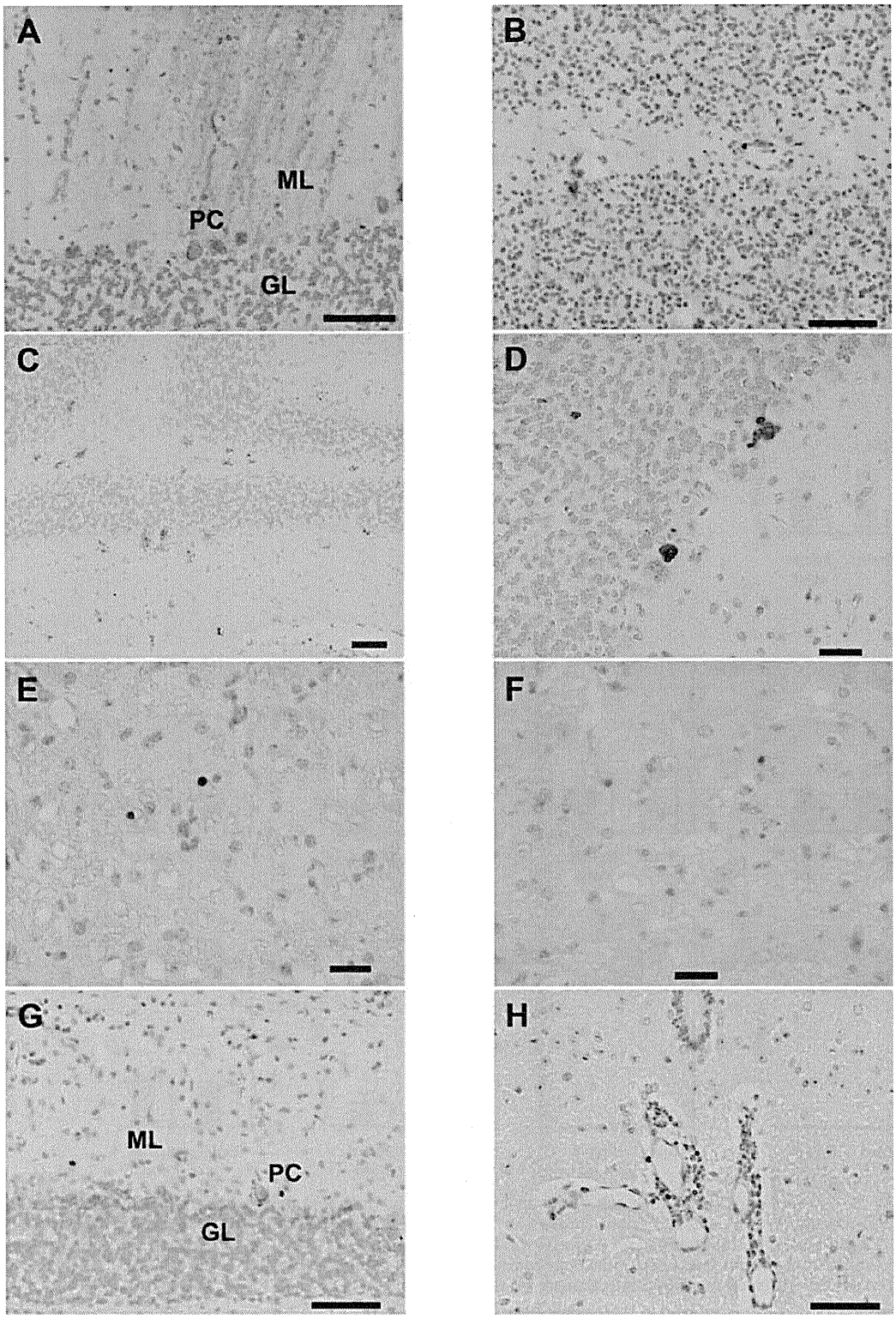

Fig. 4. Immunohistochemistry of the brains of mice infected with CVS-11. Mice intramuscularly inoculated 10^7 FFU of CVS-11 into the left hind limb were sacrificed on day 7 pi. The sections were stained with anti-P (A), anti-CD3 (B), and anti-Iba1 (C) antibodies. The apoptotic nerve cells were detected by TUNEL assay (D). Rat monoclonal [CB5.4] antibody to perforin was used to stain perforin in the cerebellar peduncle (E) and the spinal cord (F). The cerebellum (G) and the spinal cord (H) were stained for granzymes using biotinylated anti-mouse granzyme B antibody. GL, granular layer; PC, Purkinje cells; ML, molecular layer. The black bar indicates 50 μm (A, B, C, G, H) and 20 μm (D, E, F).

fect laboratory mice via a peripheral route and induces fatal infection with symptoms similar to those observed after infection with street viruses.

CVS-11, a derivative of CVS, shows high pathogenicity in mice. Peripheral inoculation of this particular strain results in dissemination of the virus to not only

the spinal cord but also the brain, leading to the death of infected animals (16,17). By comparing the CNS infections induced by pathogenic CVS-11 and apathogenic Pasteur Virus (PV) strains, Baloul and Lafon suggested that the neurovirulent RABV strains could evade the immunological attack by inducing Fas ligand (FasL)-mediated apoptosis in the protective T lymphocytes (4,5). No apparent infiltration of inflammatory cells was observed in the CNS of mice infected with the CVS-11 strain. Pathological examination performed using yellow fluorescent protein showed very limited changes in the CNS of mice infected with CVS-11, as reported by Scott et al. (18). However, Theerasurakarn and Ubol (19) reported extensive apoptosis in the brain cells of adult immunocompetent mice infected with CVS-11. In this study, apoptotic Purkinje cells as well as infiltration of CD3 lymphocytes and microglial cells were observed in infected mice.

Extensive up-regulation of genes associated with innate immunity in mice infected with the CVS-11 strain supported the results of cytokine and histopathological analyses. Canonical pathway analysis confirmed the activation of IFN signaling pathways. These findings were in good agreement with those reported previously using more attenuated CVS strains such as CVS-F3 and CVS-B2c. The differences with regard to the induction of inflammation in the CNS and up-regulation of innate immune response genes may be partly attributed to the difference in passage history of the CVS strains maintained in different laboratories.

The IL-6 gene in the CNS of CVS-11-infected mice was found to be up-regulated. Baloul and Lafon reported that the infection with a highly pathogenic CVS strain but not with an attenuated PV strain transiently increased the expression of the IL-6 gene (4). They also suggested that the up-regulation of IL-6, a neuroprotective agent, by CVS facilitated virus progression and limited inflammation, preserving neuron integrity. This allowed the neuroinvasive virus (CVS) to evade the immune responses and propagate through the CNS to the brain, resulting in the death of infected mice (4). This suggests that CVS-11 is also a highly pathogenic CVS strain.

Interestingly, perforin and granzyme genes were highly expressed in both the brain and spinal cord, whereas FasL was not considerably up-regulated. Baloul et al. (5) observed elevated expression of FasL in mice infected with the highly pathogenic CVS-11 strain but not with attenuated PV. Elimination of migrating CD3 T lymphocytes from the CNS by Fas/FasL-mediated apoptosis was implicated in the progression of fatal neurological diseases caused by pathogenic CVS-11. In this study, however, the extent of FasL up-regulation was marginal. This could be because we did not measure FasL expression in tissues obtained on day 5 pi, when the maximum level of FasL mRNA was detected by Baloul et al. (5). Histologically, most CD3 T lymphocytes showed apoptotic changes. This finding is consistent with that reported by Kojima et al. (12).

The presence of perforin and granzymes in both apoptotic neural cells and CD3 T lymphocytes strongly suggested that apoptosis was induced in these cells by mechanisms involving perforin and granzymes. Perforin and granzymes are effector molecules of CTL and natural killer (NK) cells. Target cells recognized by these effector cells are killed by apoptosis induced by perforin in association with granzymes (20,21). Some CTL could regulate T cell responses by inducing apoptosis in T lymphocytes directed to self antigens. Therefore, apoptosis was likely induced in both Purkinje cells and CD3 T lymphocytes by perforin and granzymes secreted by a particular population of T lymphocytes. Activation of IL-15 signaling pathway also suggested the involvement of activated T lymphocytes in the apoptotic mechanism.

Unlike FasL, perforin and granzymes played a major role in inducing apoptosis. Since host animals are thought to induce apoptosis of neurons to restrict the spread of the virus, strong induction of apoptosis in the neural cells is one of the important characteristic features of attenuated RABV. In contrast, induction of apoptosis in CD3 T lymphocytes is considered a key strategy of virulent viruses to evade the immune responses in the CNS and neural networks and reside in the host body. Taken together, our results suggest that both features of highly attenuated RABV caused apoptosis of neuronal cells and inhibited viral spread into the CNS, and neurovirulent RABV strains evaded immunological attack by inducing apoptosis in T lymphocytes.

Morimoto et al. (22) showed that the CVS-24 strain serially passaged in BHK cells consisted of at least 2 subpopulations of variant viruses that differed in biological properties, including pathogenicity against mice. Since CVS-11 comprised quasispecies or sub-populations that have different pathogenicities and the ratio of these subpopulations varied depending on passage histories, the studies involving different stocks of CVS-11 might yield different or contradicting results. These findings suggest that data from experiments performed using viruses that belong to the same strain but have different passage histories should be analyzed carefully. It would also be interesting to investigate whether the recently identified difference in the PDZ-binding motif of the G protein between virulent and avirulent variant viruses could have contributed to the differences in pathogenicity of virus having different passage histories (23).

Further studies are warranted to investigate whether perforin and granzymes are responsible for the induction of apoptosis in both neural cells and CD3 T lymphocytes.

Acknowledgments This study was supported by the Health and Labour Science Research grant from the Ministry of Health, Labour and Welfare of Japan.

Conflict of interest None to declare.

REFERENCES

1. Lyles, D.S. and Rupprecht, C.E. (2007): Rhabdoviridae. p. 1363–1408. Knipe, D.M., Howley, P.M., Griffin, D.E., et al. (ed.), Field's Virology. Lippincott Williams & Wilkins, Philadelphia, Pa.
2. Plotkin, S.A. (2000): Rabies. Clin. Infect. Dis., 30, 4–12.
3. Iwata, M., Unno, T., Minamoto, N., et al. (2000): Rabies virus infection prevents the modulation by alpha(2)-adrenoceptors, but not muscarinic receptors, of Ca(2+) channels in NG108–15 cells. Eur. J. Pharmacol., 404, 79–88.
4. Baloul, L. and Lafon, M. (2003): Apoptosis and rabies virus neuroinvasion. Biochimie, 85, 777–788.

5. Baloul, L., Camelo, S. and Lafon, M. (2004): Up-regulation of Fas ligand (FasL) in the central nervous system: a mechanism of immune evasion by rabies virus. J. Neurovirol., 10, 372–382.
6. Park, C.H., Kondo, M., Inoue, S., et al. (2006): The histopathogenesis of paralytic rabies in six-week-old C57BL/6J mice following inoculation of the CVS-11 strain into the right triceps surae muscle. J. Vet. Med. Sci., 68, 589–595.
7. Hooper, D.C., Morimoto, K., Bette, M., et al. (1998): Collaboration of antibody and inflammation in clearance of rabies virus from the central nervous system. J. Virol., 72, 3711–3719.
8. Dietzschold, B., Wunner, W.H., Wiktor, T.J., et al. (1983): Characterization of an antigenic determinant of the glycoprotein that correlates with pathogenicity of rabies virus. Proc. Natl. Acad. Sci. USA, 80, 70–74.
9. Dietzschold, B., Wiktor, T.J., Trojanowski, J.Q., et al. (1985): Differences in cell-to-cell spread of pathogenic and apathogenic rabies virus in vivo and in vitro. J. Virol., 56, 12–18.
10. Inoue, S., Sato, Y., Hasegawa, H., et al. (2003): Cross-reactive antigenicity of nucleoproteins of lyssaviruses recognized by a monospecific antirabies virus nucleoprotein antiserum on paraffin sections of formalin-fixed tissues. Pathol. Int., 53, 525–533.
11. Hotta, K., Motoi, Y., Okutani, A., et al. (2007): Role of GPI-anchored NCAM-120 in rabies virus infection. Microbes Infect., 9, 167–174.
12. Kojima, D., Park, C.H., Satoh, Y., et al. (2009): Pathology of the spinal cord of C57BL/6J mice infected with rabies virus (CVS-11 strain). J. Vet. Med. Sci., 71, 319–324.
13. Kojima, D., Park, C.H., Tsujikawa, S., et al. (2010): Lesions of the central nervous system induced by intracerebral inoculation of BALB/c mice with rabies virus (CVS-11). J. Vet. Med. Sci., 72, 1011–1016.
14. Miyamoto, K. and Matsumoto, S. (1967): Comparative studies between pathogenesis of street and fixed rabies infection. J. Exp. Med., 125, 447–456.
15. Yan, X., Prosniak, M., Curtis, M.T., et al. (2001): Silver-haired bat rabies virus variant does not induce apoptosis in the brain of experimentally infected mice. J. Neurovirol., 7, 518–527.
16. Coulon, P., Derbin, C., Kucera, P., et al. (1989): Invasion of the peripheral nervous systems of adult mice by the CVS strain of rabies virus and its avirulent derivative AvO1. J. Virol., 63, 3550–3554.
17. Jackson, A.C. and Reimer, D.L. (1989): Pathogenesis of experimental rabies in mice: an immunohistochemical study. Acta Neuropathol., 78, 159–165.
18. Scott, C.A., Rossiter, J.P., Andrew, R.D., et al. (2008): Structural abnormalities in neurons are sufficient to explain the clinical disease and fatal outcome of experimental rabies in yellow fluorescent protein-expressing transgenic mice. J. Virol., 82, 513–521.
19. Theerasurakarn, S. and Ubol, S. (1998): Apoptosis induction in brain during the fixed strain of rabies virus infection correlates with onset and severity of illness. J. Neurovirol., 4, 407–414.
20. Andersen, M.H., Schrama, D., Thor Straten, P., et al. (2006): Cytotoxic T cells. J. Invest. Dermatol., 126, 32–41.
21. Rousalova, I. and Krepela, E. (2010): Granzyme B-induced apoptosis in cancer cells and its regulation (review). Int. J. Oncol., 37, 1361–1378.
22. Morimoto, K., Hooper, D.C., Carbaugh, H., et al. (1998): Rabies virus quasispecies: implications for pathogenesis. Proc. Natl. Acad. Sci. USA, 95, 3152–3156.
23. Prehaud, C., Wolff, N., Terrien, E., et al. (2010): Attenuation of rabies virulence: takeover by the cytoplasmic domain of its envelope protein. Sci. Signal., 3, ra5.

THE JOURNAL OF IMMUNOLOGY

High Clonality of Virus-Specific T Lymphocytes Defined by TCR Usage in the Brains of Mice Infected with West Nile Virus

Kazutaka Kitaura, Yoshiki Fujii, Daisuke Hayasaka, Takaji Matsutani, Kenji Shirai, Noriyo Nagata, Chang-Kweng Lim, Satsuki Suzuki, Tomohiko Takasaki, Ryuji Suzuki and Ichiro Kurane

J Immunol 2011;187;3919-3930; Prepublished online 9 September 2011;
doi:10.4049/jimmunol.1100442
http://www.jimmunol.org/content/187/8/3919

The Journal of Immunology is published twice each month by
The American Association of Immunologists, Inc.,
9650 Rockville Pike, Bethesda, MD 20814-3994.

Print ISSN: 0022-1767 Online ISSN: 1550-6606.

High Clonality of Virus-Specific T Lymphocytes Defined by TCR Usage in the Brains of Mice Infected with West Nile Virus

Kazutaka Kitaura,*,†,‡ Yoshiki Fujii,*,† Daisuke Hayasaka,§ Takaji Matsutani,¶ Kenji Shirai,*,†,‡ Noriyo Nagata,‖ Chang-Kweng Lim,† Satsuki Suzuki,# Tomohiko Takasaki,† Ryuji Suzuki,* and Ichiro Kurane†,‡

It has been reported that brain-infiltrating T lymphocytes play critical roles in the clearance of West Nile virus (WNV) from the brains of mice. We characterized brain-infiltrating T lymphocytes by analyzing the TCR α- and β-chain repertoires, T cell clonality, and CDR3 sequences. $CD3^+CD8^+$ T cells were localized in the WNV-infected brains. The expression of CD3, CD8, CD25, CD69, perforin, and granzymes positively correlated with viral RNA levels, and high levels of expression of IFN-γ, TNF-α, and IL-2 were detected in the brains, suggesting that Th1-like cytotoxic $CD8^+$ T cells are expanded in the brains in response to WNV infection. The brain-infiltrating T lymphocytes dominantly used TCR genes, VA1-1, VA2-1, VB5-2, and VB8-2, and exhibited a highly oligoclonal TCR repertoire. Interestingly, the brain-infiltrating T lymphocytes had different patterns of TCR repertoire usages among WNV-, Japanese encephalitis virus-, and tick-borne encephalitis virus-infected mice. Moreover, $CD8^+$ T cells isolated from the brains of WNV-infected mice produced IFN-γ and TNF-α after in vitro stimulation with peritoneal cells infected with WNV, but not with Japanese encephalitis virus. The results suggest that the infiltrating $CD8^+$ T cells were WNV-specific, but not cross-reactive among flaviviruses. T cells from the WNV-infected brains exhibited identical or similar CDR3 sequences in TCRα among tested mice, but somewhat diverse sequences in TCRβ. The results indicate that WNV-specific $CD3^+$ $CD8^+$ T cells expanding in the infected brains are highly oligoclonal, and they suggest that TCR α-chains play a dominant and critical role in Ag specificity of WNV-specific T cells. *The Journal of Immunology*, **2011, 187: 3919–3930.**

West Nile virus (WNV) is a member of the Flaviviridae family and causes a range of illnesses from mild fever to acute flaccid paralysis and lethal encephalitis in humans. Approximately 20–30% of infected individuals develop flu-like clinical manifestations characterized as West Nile fever, and about 1 in 150 cases is accompanied by severe neurologic disease, such as cognitive dysfunction, ocular manifestations, meningitis, encephalitis, and flaccid paralysis (1–3). West Nile fever was endemic in the Middle East, Europe, and Africa before the mid-1990s, but has since spread throughout the world, including the Americas (4). However, vaccines or specific therapies for WNV are unavailable for humans. Moreover, the pathogenesis of WNV encephalitis is not clear, especially the reasons why most of the symptomatic cases demonstrate acute febrile illness but some develop severe encephalitis.

$CD8^+$ cytotoxic T cells play essential roles in controlling WNV infection (5) and protection against WNV encephalitis (6). Previously, we have demonstrated the existence of Ag-specific T cells in the brains of C3H mice infected with Japanese encephalitis virus (JEV), which is closely related to WNV (7). In mice infected with flaviviruses, Ag-specific T lymphocytes infiltrating into the CNS mediate the clearance of virus, preventing encephalitis. However, little information regarding Ag specificity and diversity of the CNS-infiltrating T cells is available. Immune responses against virus infections are initiated by specific recognition of a viral Ag presented on an MHC by a TCR. Functional TCR α- and β-chains genes are generated by somatic gene rearrangements of germline-encoded V(D)J and constant gene segments. The Ag specificity and diversity of the TCR depends mainly on CDR3, formed by nucleotide addition/insertion during the gene rearrangements (8) that contact directly with an Ag peptide on MHC (9). Many investigations with quantitative and qualitative analyses of TCR repertoires and CDR3 sequences have contributed to the elucidation of pathological conditions and/or immunological dynamics in infectious disease research (7), pathogenesis of autoimmune diseases (10–12), and/or physiological analysis (13, 14). Additionally, neutralizing Abs induced by WNV partially protect against JEV infection (15). The immunological cross-reaction between closely related flaviviruses raised the question of whether

*Department of Rheumatology and Clinical Immunology, Clinical Research Center for Allergy and Rheumatology, Sagamihara National Hospital, National Hospital Organization, Kanagawa 228-0815, Japan; †Department of Virology 1, National Institute of Infectious Diseases, Tokyo 162-8640, Japan; ‡Department of Infection Biology, Institute of Basic Medical Sciences, University of Tsukuba, Ibaraki 305-8575, Japan; §Department of Virology, Institute of Tropical Medicine, Nagasaki University, Nagasaki 852-8523, Japan; ¶Laboratory of Immune Regulation, Wakayama Medical University, Osaka, 567-0085, Japan; ‖Department of Pathology, National Institute of Infectious Diseases, Tokyo 208-0011, Japan; and #Section of Biological Science, Research Center for Odontology, Nippon Dental University School of Life Dentistry at Tokyo, Tokyo 102-8159, Japan

Received for publication February 14, 2011. Accepted for publication July 27, 2011.

This work was supported in part by Grants-in-Aid for Research on Emerging and Re-emerging Infectious Diseases from the Ministry of Health, Labor, and Welfare, Japan (Grants H20-shinkou-ippan-013 and H20-shinkou-ippan-015) as well as by Grant-in-Aid for Challenging Exploratory Research 23659237 from the Japan Society for the Promotion of Science.

Address correspondence and reprint requests to Dr. Ichiro Kurane, Department of Virology 1, National Institute of Infectious Diseases, 1-23-1 Toyama, Shinjuku-ku, Tokyo 162-8640, Japan. E-mail address: kurane@nih.go.jp

Abbreviations used in this article: BSL, biosafety level; IHC, immunohistochemical; JEV, Japanese encephalitis virus; MCA, TCR α-chain C region-specific primer; MCB, TCR β-chain C region-specific primer; PEC, peritoneal cell; qPCR, quantitative real-time RT-PCR; TBEV, tick-borne encephalitis virus; TCRAV, TCR α-chain variable; TCRBV, TCR β-chain variable; TCRV, TCR V region; WNV, West Nile virus.

www.jimmunol.org/cgi/doi/10.4049/jimmunol.1100442

brain-infiltrating T lymphocytes use identical or similar TCR repertoires among these closely related flaviviruses.

To characterize the brain-infiltrating T lymphocytes in WNV-infected mice, we performed immunohistochemical (IHC) and quantitative real-time RT-PCR (qPCR) analyses for T cell-related surface molecules, cytokines, chemokines, and cytotoxic granules. The results demonstrated that Th1-like cytotoxic $CD8^+$ T cells accumulated in the brains. Next, to disclose Ag specificity and diversity in the brain-infiltrating T lymphocytes, we analyzed the TCR repertoires and TCR clonotypes in the brains of mice infected with WNV, JEV, and tick-borne encephalitis virus (TBEV). The results indicated that T cells accumulated in the mice brains had a distinct TCR repertoire among WNV, JEV, and TBEV and exhibited high oligoclonality. Furthermore, we performed in vitro stimulation assays by coculturing T cells isolated from WNV-infected mouse brains with peritoneal cells (PECs) obtained from different strains of mice that were infected with either WNV or JEV. These T cells produced IFN-γ and TNF-α in response to WNV-infected PECs with a syngeneic MHC haplotype. The present study provides important information about the Ag specificity and diversity of brain-infiltrating T lymphocytes in flavivirus-infected mice.

Materials and Methods

Virus

The NY99-6922 strain of WNV (GenBank accession no. AB185915; http://www.ncbi.nlm.nih.gov/genbank and the JaTH160 strain of JEV (GenBank accession no. AB269326) were used in this study. The WNV was prepared from the conditioned medium of Vero cells that were infected with a previously prepared virus stock (15). Vero cells were maintained in Eagle's MEM (Nissui Pharmaceutical, Tokyo, Japan) containing 10% FCS. The virus titer was 1.4×10^5 PFU/ml. JEV was prepared as described previously (7) with a virus titer of 1×10^{10} PFU/ml. The experiments using live viruses were performed in a biosafety level (BSL) 3 laboratory of the National Institute of Infectious Diseases, Japan, according to standard BSL3 guidelines. The Oshima 5-10 strain of TBEV (GenBank accession no. AB062063) (16) was also used in this study. The virus was prepared from the conditioned medium of baby hamster kidney cells infected with a previously prepared virus stock (17). Baby hamster kidney cells were maintained in Eagle's MEM containing 8% FCS. Experiments using live TBEV were performed in a BSL3 laboratory of the Tokyo Metropolitan Institute for Neuroscience according to standard BSL3 guidelines.

Mice

C3H/HeNJcl (H-2^k), C57BL/6JJcl (H-2^b), and BALB/cAJcl (H-2^d) female mice were purchased from CLEA Japan (Tokyo, Japan) and kept in a specific pathogen-free environment. All animal experiments were done according to the relevant ethical requirements and with approval from the committees for animal experiments at the National Institute of Infectious Diseases and the Tokyo Metropolitan Institute for Neuroscience, Japan.

Virus challenges

Seven-week-old C3H/HeNJcl female mice were injected i.p. with the $30 \times LD_{50}$ (1.3×10^3 PFU/0.5 ml) WNV and the $100 \times LD_{50}$ (1.2×10^4 PFU/0.5 ml) JEV or PBS alone (mock infection). Four, 7, and 10 days later, WNV-infected mice were sacrificed under general anesthesia. Ten days later, JEV-infected mice were sacrificed under general anesthesia. In TBEV infection, 7-wk-old C3H/HeNJcl female mice were injected s.c. with 1.0×10^3 PFU/0.5 ml TBEV or PBS. Thirteen days later, mice were sacrificed under general anesthesia.

Histological and IHC analyses

Brains were excised for use in histological and IHC examinations. Tissue samples were fixed overnight at 4°C with paraformaldehyde-lysine-periodate, washed with PBS, and immersed in 5% sucrose/PBS for 1 h, in 15% sucrose/PBS for 3 h, and in 30% sucrose/PBS overnight at 4°C. Samples were embedded in Tissu Mount (Chiba Medical, Saitama, Japan) and quick-frozen in a mixture of acetone and dry ice. For histochemical staining, 6-μm cryosections were air-dried on poly-L-lysine–coated glass slides and were stained with H&E. For IHC analyses, cryosections were stained with anti-mouse CD3ε (145-2C11; BD Pharmingen, San Diego, CA), CD4 (GK5.1; BD Pharmingen), and CD8α (53-6.7; BD Pharmingen) mAbs. In short, glass slides were overlaid with PBS containing blocking reagents (a 1:20 dilution of normal goat serum or normal rabbit serum, 0.025% Triton X-100 [Wako Pure Chemicals, Osaka, Japan], and 5% BSA [Sigma-Aldrich, St. Louis, MO]) and incubated for 30 min at room temperature. The mAbs were loaded onto the glass slides and incubated for 1 h at room temperature. After washing with PBS (three times for 5 min), each section was treated with a secondary Ab (biotinylated goat anti-hamster IgG Ab or biotinylated rabbit anti-rat IgG Ab) at room temperature for 1 h and then with avidin–biotin complex for 30 min, followed by 3,3′-diaminobenzidine staining (0.06% 3,3′-diaminobenzidine, 0.03% H_2O_2 in 0.1 M Tris-HCl buffer [pH 7.6]; Wako Pure Chemicals). Finally, the glass slides were counterstained with hematoxylin to visualize nuclei.

Isolation of total RNA from tissues

Fresh brains and spleens infected with WNV or TBEV were excised intact and immediately submerged in RNAlater RNA stabilization reagent (Qiagen, Hilden, Germany) (18). Total RNA was isolated using the RNeasy Lipid Tissue Mini Kit (Qiagen) according to the manufacturer's instructions.

Quantitative estimation of the expression of immune-related genes and WNV RNA in brains and spleens

Expression levels of mRNA for immune-related genes including T cell-related CD Ags, cytokines, chemokines, chemokine receptors, and cytotoxic granules were measured by qPCR using a LightCycler apparatus (Roche Diagnostics, Basel, Switzerland). Previously demonstrated primer pairs specific for GAPDH, CD3, CD4, CD8, IFN-γ, TNF-α, IL-2, IL-4, IL-5, CCL5, CXCL10, and CXCR3 were used in this study (7, 19). Other primer pairs (CCR5, perforin, granzyme A, granzyme B, CD25 [IL-2Rα], and CD69) were designed for this study (Table I). IL-10–specific primers were purchased from Takara Bio (Otsu, Japan). Freshly isolated RNA from the spleens and brains of WNV- or mock-infected mice ($n = 5$) was converted to cDNA using a PrimeScript RT reagent kit (Takara Bio) according to the manufacturer's instructions. The PCR reaction was performed using SYBR Premix TaqII (Takara Bio) for SYBR Green I and was carried out in a 20-μl volume containing 2 μl cDNA template originating from 50 ng total RNA, 0.4 μl each 10 μM forward and reverse primers, and 10 μl SYBR Premix TaqII. After an initial denaturation step at 95°C for 10 s, temperature cycling was initiated. Each cycle consisted of 95°C for 5 s and 60°C for 30 s, and the fluorescence was read at the end of this second step. In total, 40 cycles for GAPDH and 50 cycles for other primer sets were performed accordingly. Melting curve analysis was performed immediately after amplification at a linear temperature transition rate of 0.1°C/s from 65°C to 95°C with continuous fluorescence acquisition. The absolute copy number of each gene was calculated by using a standard curve generated by serial dilution of the recombinant plasmid DNA encoding gene of interest, ranging from 10^1 to 10^8 copies. Calculated copy numbers were normalized based on the copy numbers of the housekeeping gene GAPDH.

Table I. Sequences of qPCR primers

Targets	Forward Primer (5′–3′)	Reverse Primer (5′–3′)
CCR5	ATATGCAAAGGGACGGACAC	GCAAGAAGCGACTTTATGGC
IL-10	GACCAGCTGGACAACATACTGCTAA	GATAAGGCTTGGCAACCCAAGTAA
Perforin	GCCTGGTACAAAAACCTCCA	AGGGCTGTAAGGACCGAGAT
Granzyme A	CCTGAAGGAGGCTGTGAAAG	GAGTGAGCCCCAAGAATGAA
Granzyme B	CCATCGTCCCTAGAGCTGAG	TTGTGGAGAGGGCAAACTTC
CD25	AAGATGAAGTGTGGGAAAACGG	GGGAAGTCTGTGGTGGTTATGG
CD69	AGGATCCATTCAAGTTTCTATCCC	CAACATGGTGGTCAGATGATTCC

The viral RNA levels of WNV were examined with envelope-specific forward and reverse primers (5′-TCAGCGATCTCTCCACCAAAG-3′ and 5′-GGGTCAGCACGTTTGTCATTG-3′) and a dual fluorophore-labeled probe (5′-CFSE-TGCCCGACCATGGGAGAAGCTC-TAMRA-3′) using a Prism 7000 sequence detection system (Applied Biosystems, Foster, CA). A TaqMan Ez RT-PCR kit (Applied Biosystems) was used according to the manufacturer's instructions. A total reaction mixture of 25 μl containing 50 ng total RNA was incubated at 48°C for 30 min for reverse transcription and then at 95°C for 10 min for inactivation of reverse transcriptase and initial denaturation. PCR was carried out for 40 cycles at 95°C for 15 s and 57°C for 1 min, and the fluorescence was read at the final PCR round. The copy number of each sample was determined on the basis of a standard curve created with a serial dilution of in vitro-synthesized WNV RNA ranging from 10^1 to 10^8 copies, provided by Dr. Soichi Nukuzuma (Kobe Institute of Health, Kobe, Hyogo, Japan).

TCR repertoire analysis

TCR repertoire analysis was performed with WNV- and TBEV-infected mice samples (n = 5) by an adaptor ligation-mediated PCR and microplate hybridization assay method (20–22). Briefly, isolated total RNA was converted to double-stranded cDNA using a SuperScript cDNA synthesis kit (Invitrogen, Carlsbad, CA) according to the manufacturer's instructions, except that a specific primer (BSL-18E) was used (22). The P10EA/P20EA adaptors were ligated to the 5′ end of the cDNA and this adaptor-ligated cDNA was cut with SphI. PCR was performed with TCR α-chain C region-specific (MCA) 1 or TCR β-chain C region-specific primers (MCB) 1 and P20EA. The second PCR was performed with MCA2 or MCB2 and P20EA. The third PCR was performed using both P20EA and 5′-biotinylated MCA3 or MCB3 primer for biotinylation of PCR products.

Ten picomoles of amino-modified oligonucleotides specific for the TCR α-chain variable (TCRAV) and TCR β-chain variable (TCRBV) segments were immobilized onto carboxylate-modified 96-well microplates with water-soluble carbodiimide. Prehybridization and hybridization were performed in GMCF buffer (0.5 M Na_2HPO_4 [pH 7.0], 1 mM EDTA, 7% SDS, 1% BSA, and 7.5% formamide) at 47°C. One hundred microliters of the denatured 5′-biotinylated PCR products was mixed with the equivalent volume of 0.4 N NaOH/10 mM EDTA, and the mixture was added to 10 ml GMCF buffer. One hundred microliters of hybridization solution was used in each well of the microplate containing immobilized oligonucleotide probes specific for V segments. After hybridization, wells were washed four times with washing buffer (2× SSC, 0.1% SDS) at room temperature. Plates were then incubated at 37°C for 10 min for stringency washing. After washing four times with the same washing buffer, 200 μl TB-TBS buffer (10 mM Tris-HCl, 0.5 M NaCl [pH 7.4], 0.5% Tween 20, and 0.5% blocking reagent; Roche Diagnostics) was added to block nonspecific binding. Next, 100 μl 1:2000 diluted alkaline phosphatase-conjugated streptavidin in TB-TBS was added, and the sample was incubated at 37°C for 30 min. Plates were washed six times in T-TBS (10 mM Tris-HCl, 0.5 M NaCl [pH 7.4], 0.5% Tween 20). For color development, 100 μl substrate solution (4 mg/ml p-nitrophenylphosphate [Sigma Aldrich] in 10% diethanolamine [pH 9.8]) was added, and absorbance was determined at 405 nm. The ratio of the hybridization intensity of each TCR V region (TCRV)-specific probe to that of a TCR C region-specific probe (V/C value) was determined using the TCR cDNA concentrated samples that contained the corresponding TCRV segment and the universal TCR constant segment, respectively. Absorbance obtained with each TCRV-specific probe was divided by the corresponding V/C value. The relative frequency was calculated based on the corrected absorbances using the formula: relative frequency (%) = (corrected absorbance of TCRV-specific probe/sum of corrected absorbances of TCRV-specific probes) × 100.

T cell clonality analysis with CDR3 size spectratyping

The level of T cell clonality was evaluated in samples from WNV- and TBEV-infected mice (n = 5) using a CDR3 size spectratyping method (23). PCR was performed for 30 cycles in a 20 μl volume under the same conditions as described above. The PCR mixture consisted of 1 μl 1:20 or 1:50 diluted second PCR product, 0.1 μM 5′-Cy5 MCA3/MCB3 primer, and 0.1 μM primer specific for each variable segment. Two microliters 1:20 diluted PCR product was analyzed with the CEQ8000 genetic analysis system (Beckman Coulter, Fullerton, CA). The spleens of mock-infected mice were used as normal controls showing a Gaussian distribution pattern with multiple peaks.

Determination of CDR3 nucleotide sequences

PCR was performed with 1 μl 1:20 diluted second PCR product, using a forward primer specific for the V region and a reverse primer specific for the C region (MCA4 or MCB4) under the conditions described above. The primers used in this study were as follows: VA1-1, 5′-AGACTCCCAGCCCAGTGACT-3′; VA2-1, 5′-TGCAGTTATGAGGACAGCACTT-3′; VB5-2, 5′-GGATTCCTACCCAGCAGATTC-3′; and VB8-2, 5′-GGCTACCCCCTCTCAGACAT-3′. After elution from agarose gels, PCR products were cloned into the pGEM-T Easy Vector (Promega, Madison, WI). The recombinant plasmid DNA was transfected into DH5α competent cells. Sequence reactions were performed with the GenomeLab DTCS Quick Start Kit (Beckman Coulter) and analyzed by the CEQ8000 genetic analysis system (Beckman Coulter). In total, 64 clones from each sample of WNV- and TBEV-infected mouse brains (n = 5) were examined in this experiment.

In vitro stimulation of T cells from WNV-infected mouse brain

WNV- or JEV-infected C3H/HeN mice (n = 8) were sacrificed under general anesthesia on day 10 postinfection, and brains were removed. Brains were kept on ice in RPMI 1640 containing 10% FCS and homogenized gently by pressing through a 100-μm mesh tissue strainer (BD Pharmingen). Homogenates were then centrifuged at 400 × g for 10 min, and cell pellets were resuspended in 5 ml RPMI 1640 and layered over 5 ml Lympholyte-M (Cedarlane Laboratories, Hornby, ON, Canada) before centrifugation at 1000 × g for 20 min at 22°C. Next, the isolated lymphocyte pool was washed twice and resuspended in MACS buffer (Ca^+- and Mg^+-free PBS, 2 mM EDTA, and 0.5% BSA) and incubated with anti-CD4 and/or anti-CD8 MACS beads (Miltenyi Biotec, Auburn, CA) at 4°C for 15 min. Cell suspensions were diluted 20 times in

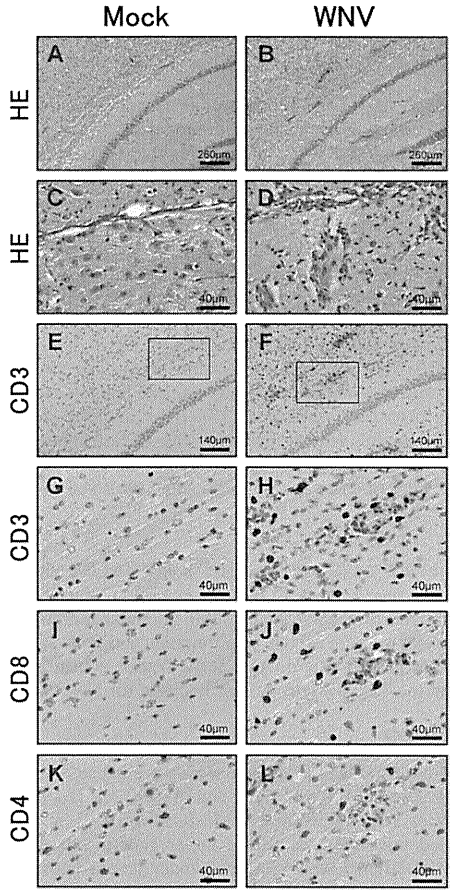

FIGURE 1. Histopathological study and IHC analysis of $CD3^+$, $CD8^+$, and $CD4^+$ cells in WNV-infected mouse brain. Representative photomicrographs of brain sections from mock-infected or WNV-infected mice at day 10 postinfection, stained with H&E (*A–D*) and CD3, CD4, and CD8 (*E–L*). Neuronal degeneration and inflammatory cell infiltration in hippocampus and perivascular areas are shown in WNV-infected mouse brains, but not those of mock-infected mice. For the IHC analysis, the localization of $CD3^+$ and $CD8^+$ cells is shown throughout the brain of WNV-infected mice, but not those of mock-infected mice (*E–J*). Alternatively, $CD4^+$ cells were detected sporadically in both WNV- and mock-infected mice (*K*, *L*). The area of higher magnifications (original magnification ×3.5) are indicated by the black boxes in *E* and *F*.

MACS buffer and centrifuged at 300 × *g* for 10 min. Cell pellets were resuspended in MACS buffer and filtered through MACS LS separation columns (Miltenyi Biotec), according to the manufacturer's protocol. Collected $CD4^+$ and/or $CD8^+$ cells were resuspended in RPMI 1640 containing 10% FCS and antibiotics (assay medium), adjusted to 2.5×10^6 cells/ml, and were used in in vitro stimulation assays. PECs were collected in 10 ml cold Ca^+- and Mg^+-free PBS, from C3H/HeN, C57BL/6j, and BALB/c mice ($n = 3$) after scarifying the mice under general anesthesia. The cells were centrifuged at 600 × *g* for 5 min, resuspended in assay medium, and counted. After infection with WNV or JEV at a multiplicity of infection of 100 PFU/cell at 37°C in 5% CO_2 for 60 min, the cells were washed twice with assay medium. The concentration of PECs was adjusted to 5.0×10^5 cells/ml, and 100 μl PEC was dispensed into flat-bottom 96-well trays (Nunc, Roskilde, Denmark). Subsequently, 100 μl 2.5×10^5 T cells from WNV- or JEV-infected C3H mouse brains was added and cultured at 37°C in 5% CO_2 for 12 h. Culture supernatant fluids were collected, and levels of IFN-γ and TNF-α were measured by ELISA (MIF00 and MTA00, respectively; R&D Systems, Minneapolis, MN) according to the manufacturer's instructions. Cells were then further cultured for 3 d and used for CDR3 analysis.

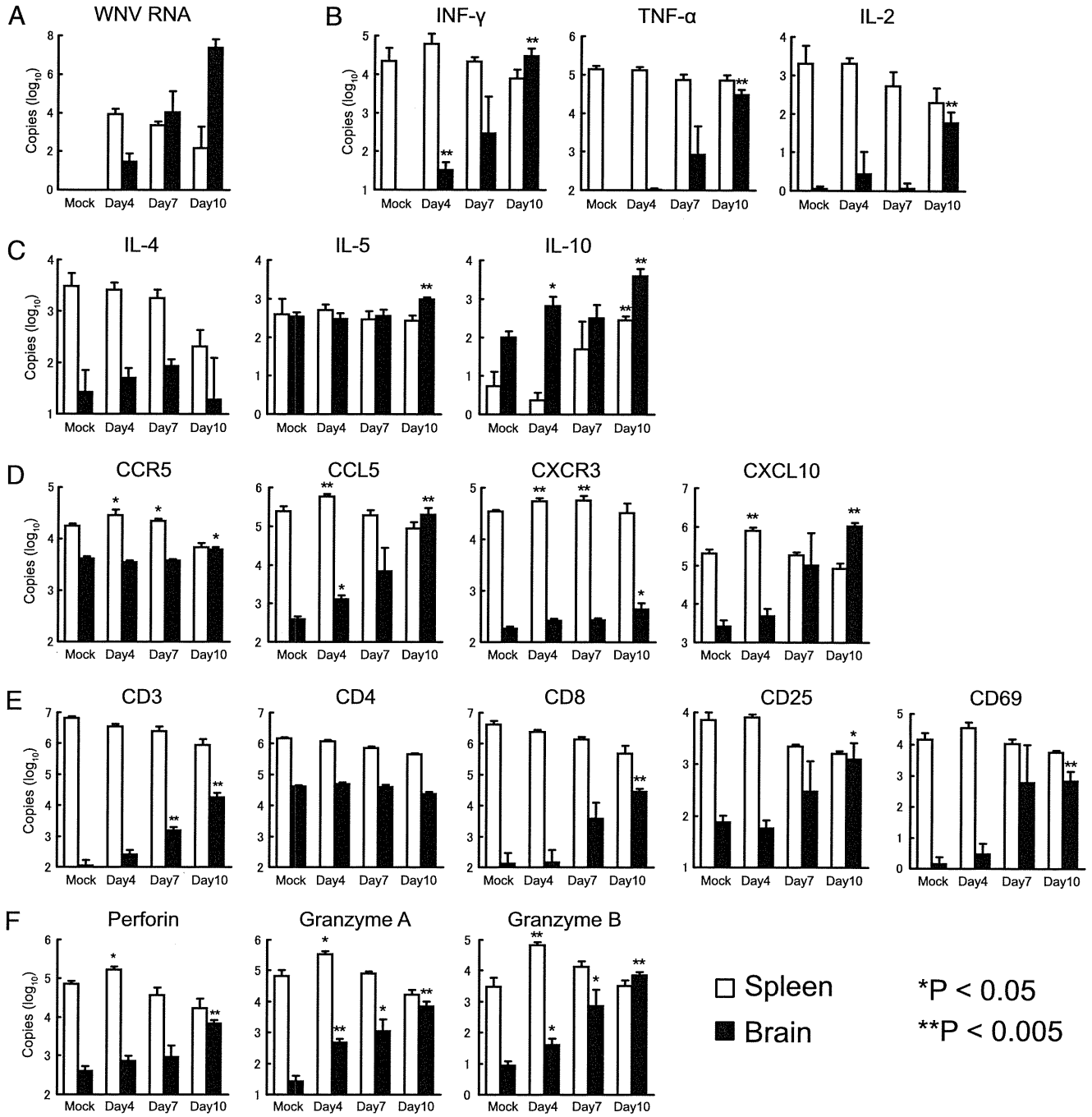

FIGURE 2. Quantification of WNV RNA and of T cell immune-related gene mRNAs by qPCR. Copy number of WNV RNA (*A*), the mRNA expression level of IFN-γ, TNF-α, and IL-2 as Th1-type cytokines (*B*), IL-4, IL-5, and IL-10 as Th2 type cytokines (*C*), CCR5, CCL5, CXCR3, and CXCL10 as chemokines and chemokine receptors (*D*), CD3, CD4, CD8, CD25 (IL-2R), and CD69 as T cell-related Ags (*E*), and perforin, granzyme A, and granzyme B as cytotoxic granules (*F*) are shown. The copy numbers per 50 ng total RNA were calibrated with GAPDH expression, except that WNV RNA was calculated from the standard density of in vitro-synthesized WNV RNA. RNA was extracted from spleens (open bars) or brains (filled bars) of mock-infected mice (Mock) or WNV-infected mice at 4, 7, and 10 d after virus inoculation. Open or filled bars and vertical error bars indicate mean ± SD of five mice. Significant differences are shown when compared with mock spleen or brain using a Student unpaired *t* test (*$p < 0.05$, **$p < 0.005$). All experiments were performed in triplicate.

Statistical analysis

Differences were statistically analyzed by a Student unpaired *t* test using StatView 5.0 for Windows (SAS Institute, Cary, NC). A p value <0.05 was determined to be statistically significant. Moreover, to assess biologically significant differences, a 5% cut-off threshold was added for TCR repertoires.

Results

Histopathological study of brains from WNV-infected mice

Brains were removed from WNV- or mock-infected mice 10 d postinfection and prepared for histopathological examinations as described in *Materials and Methods*. Representative histological changes are shown in Fig. 1*A–D*. Severe neuronal degeneration and inflammatory cell infiltration were detected in the brains from infected mice, especially in the hippocampus, perivascular tissue, and cerebral meninges. In WNV-infected mouse brains, but not in mock-infected mouse brains, $CD3^+$ and $CD8^+$ T cells were also widely detected, especially in the cerebral meninges, perivascular tissue, and hippocampus (Fig. 1*E–J*). $CD4^+$ cells were detected in brain sections both from WNV- and mock-infected mice (Fig. 1*K*, 1*L*).

Propagation of WNV and cytokine expression in brains from WNV-infected mice

The amount of WNV RNA in brains and spleens was measured by qPCR after i.p. inoculation of the virus (Fig. 2*A*). WNV RNA was first detected on day 4 in both organs. RNA levels increased largely with time in the brains, whereas they gradually decreased after day 4 in the spleens. Cytokine expression in the brains of WNV-infected mice was also measured (Fig. 2*B*, 2*C*). A temporal increase in the expression of IFN-γ, TNF-α, and IL-2 was detected in the brains of the WNV-infected mice, but not in those of mock-infected ones. IL-4, IL-5, and IL-10 expression was detected in the brains of mock-infected mice. The expression levels of IL-5 increased significantly on day 10 in WNV-infected mice. The expression of IL-10 increased on day 4 in the brains and slowly in the spleens following WNV infection. The expression levels of chemokines (CCL5 and CXCL10) and chemokine receptors (CCR5 and CXCR3) considerably increased in the brains after WNV infection (Fig. 2*D*). In particular, the expression levels of CCL5 and CXCL10 were increased >100-fold on day 10 compared with day 4. These results indicated that expression

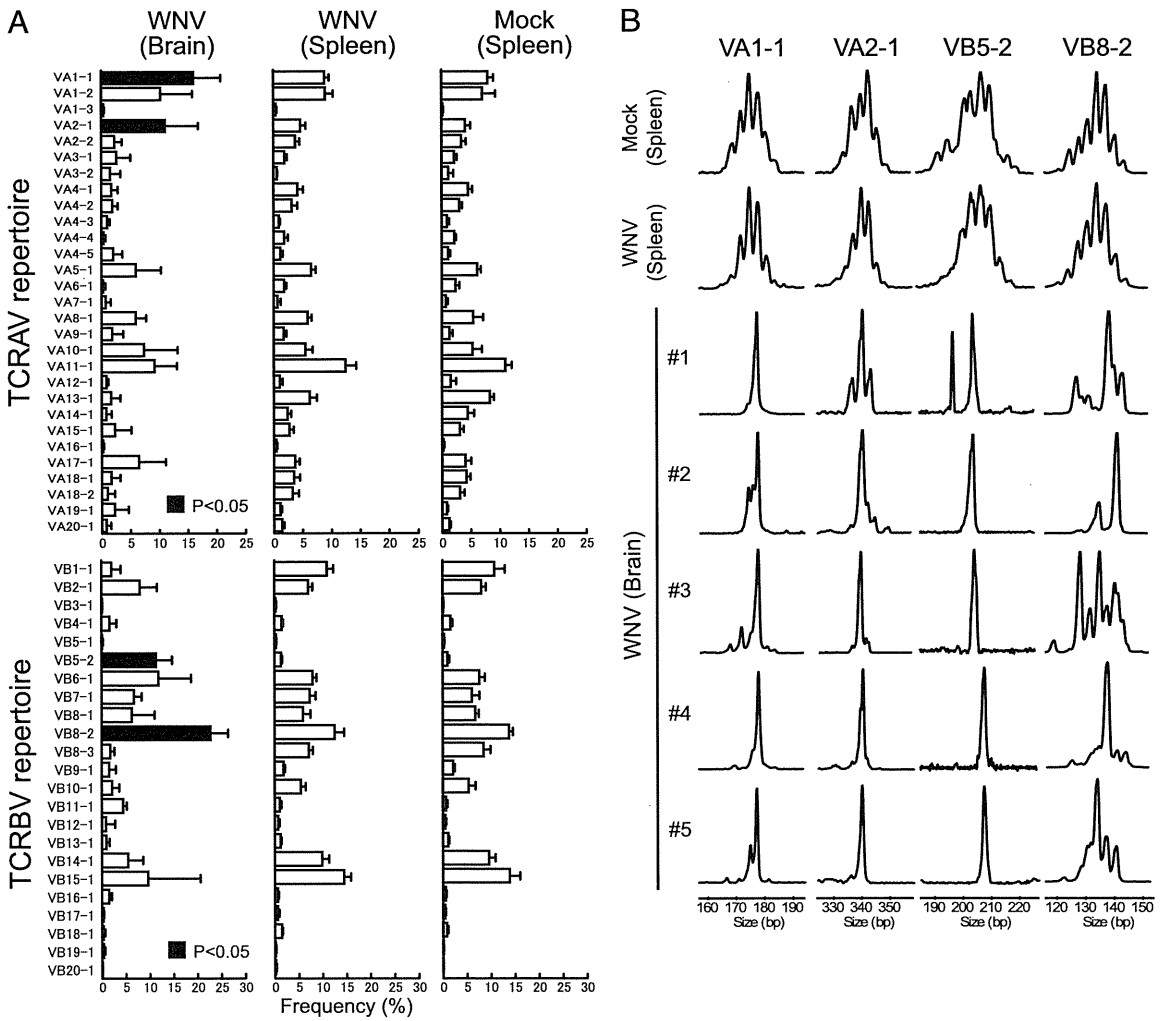

FIGURE 3. TCR repertoire analysis and CDR3 size spectratyping in spleens and brains of WNV-infected mice. *A*, TCRAV and TCRBV repertoires were analyzed by microplate hybridization assay method. The open or filled bars and horizontal bars indicate mean ± SD of frequencies in five mice. In the brains of WNV-infected mice on day 10, percentage frequencies of T cells bearing VA1-1, VA2-1, VB5-2, and VB8-2 were significantly increased compared with those of mock-infected mouse spleens ($p < 0.05$, Student unpaired *t* test, filled bars). All experiments were performed in triplicates. *B*, CDR3 size spectratyping patterns of VA1-1, VA2-1, VB5-2, and VB8-2 in five mice infected with WNV on day 10. Multiple peaks with a Gaussian distribution showing the presence of polyclonal T cells are seen in the spleen of mock-infected mice (control). The same pattern was found in the spleens of WNV-infected mice. In contrast, a single or a few peaks, signifying high levels of oligoclonality, were obtained from all VA and VB families tested in the WNV-infected brains.

levels of Th1-type cytokines and chemokines positively correlated with the propagation of WNV in the brains.

Infiltration of T cells in the brains of WNV-infected mice

To confirm the presence of brain-infiltrating T cells, expression of CD3, CD4, CD8, CD25, and CD69 was measured (Fig. 2*E*). CD3 and CD8 were expressed at low levels during the early phase of infection in WNV- and mock-infected brains. However, their expression considerably increased during the late phase of infection. CD25 and CD69 showed a similar expression pattern as CD3 and CD8. These results suggested that activated $CD3^+CD8^+$ T cells infiltrated the brains of the WNV-infected mice. CD4 transcripts were consistently detected in both WNV- and mock-infected mice. The expression of cytotoxic granule components (perforin, granzyme A, and granzyme B) was measured by qPCR (Fig. 2*F*) and found to be rapidly increased in the early stages of WNV infection in both spleens and brains, positively correlating with CD3, CD8, CD25, and CD69 expression. These results suggested that cytotoxic T lymphocytes expanded in the brains of WNV-infected mice.

TCR repertoire and clonality in brain-infiltrating T cells

TCRAV and TCRBV repertoires were analyzed from the spleens and brains of WNV- or mock-infected mice 10 d postinfection (Fig. 3*A*). The TCRAV and TCRBV repertoires were not significantly different in the spleens between the WNV- and the mock-infected mice. In contrast, the percentage frequencies of T cells bearing VA1-1, VA2-1, VB5-2, and VB8-2 were significantly higher in the brains of WNV-infected mice than in the spleens from WNV- or mock-infected mice. The expression levels of these families were increased from day 4 to day 10 in the brains (Fig. 4*A*). Expression of TCR genes was not detected in the brains from mock-infected mice. Furthermore, T cell clonality was examined by a CDR3 size spectratyping method and a significant increase in the clonality was detected in VA1-1, VA2-1, VB5-2, and VB8-2 (Fig. 3*B*). Polyclonal peak patterns were detected in the spleens of mock- and WNV-infected mice while oligoclonal or monoclonal peak patterns were detected in the brains of WNV-infected mice on day 10. Dominant peaks in VA1-1, VA2-1, and VB5-2 appeared to be identical in size among individual mice, whereas an oligoclonal peak pattern was detected in VB8-2.

Determination of CDR3 nucleotide sequences

CDR3 nucleotide sequences were determined with cDNA clones obtained from the spleen of mock-infected mice and the brains of WNV-infected mice. Predicted amino acid sequences with occurrence frequencies of the respective cDNA clones are shown in Fig 5. The cDNA clones obtained from the spleen of the mock-infected mice displayed highly diverse CDR3 sequences (data not shown), which corresponded to the results from CDR3 size spectratyping. In contrast, oligoclonal or monoclonal T cells were detected in VA1-1, VA2-1, and VB5-2 in the brains of WNV-infected mice.

In VA1-1, five clonotypes (CAVS-IG-NSGTYQRFG, CAVS-MG-NSGTYQRFG, CAVS-KG-NSGTYQRFG, CAVS-PG-NSGTYQRFG, and CAVS-MG-GYQNFYFG) were obtained from the brains of different mice (Fig. 5*A*). Interestingly, these clonotypes had only one amino acid difference in the N region. Additionally, preferential usage in AJ13 was observed in the WNV-infected brains (47 of 51 clones for mouse 1, 47 of 52 for mouse 2, 20 of 50 for mouse 3, 15 of 52 for mouse 4, and 25 of 51 for mouse 5). A similar result was also obtained from sequence analysis of VA2-1 (Fig. 5*B*). Two dominant clonotypes (CAAS-EG-GNYK-

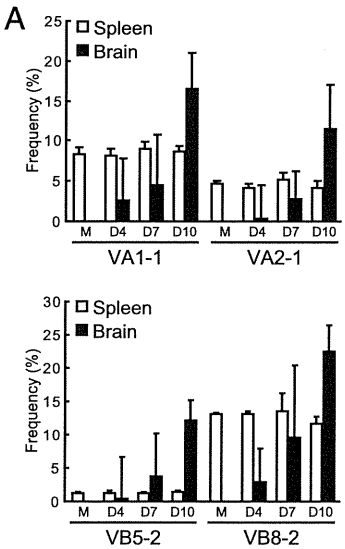

B

VA1-1

Brain	Clonal frequency	V	N	J	J gene
Day 4					
#1	1/11	CA	ASI	SGSFNKLTFG	AJ04
	1/11	CAV	MSS	TSGGNYKPTFG	AJ06
	1/11	CAVS	R	NMGYKLTFG	AJ09
	1/11	CA	VN	TNSAGNKLTFG	AJ17
	1/11	CAAS		DRGSALGRLHFG	AJ18
	1/11	CA	ASM	PGTGSNRLTFG	AJ28
	1/11	CAV	SK	NTRKLIFG	AJ37
	1/11	CAV	MT	NNAGAKLTFG	AJ39
	1/11	CAAS	PA	SGGSNAKLTFG	AJ42
	1/11	CAVS		GADRLTFG	AJ45
	1/11	CAVS	FSV	GGSNYKLTFG	AJ53
#2	1/14	CA	VSIG	NTGGLSG	AJ02
	1/14	CA	VA	NSGTYQRFG	AJ13
	1/14	CAAS	D	QGGRALIFG	AJ15
	1/14	CAA	F	GSALGRLHFG	AJ18
	1/14	CAAS	ANL	NTNTGKLTFG	AJ27
	1/14	CA	VR	PGTGSNRLTFG	AJ28
	1/14	CAA	P	LPGTGSNRLTFG	AJ28
	1/14	CAVS	MAG	NNRIFFG	AJ31
	1/14	CA	VSL	GSSGNKLIFG	AJ32
	1/14	CA	VSH	SNYQLIWG	AJ33
	1/14	CA	VTL	NNAGAKLTFG	AJ39
	1/14	CAV	RS	NTGYQNFYFG	AJ49
	1/14	CAVS	KSM	SSFSKLVFG	AJ50
	1/14	CA	VRK	GGSAKLIFG	AJ57
#3	1/12	CA	ASG	NMGYKLTFG	AJ09
	1/12	CAV		NMGYKLTFG	AJ09
	1/12	CA	AG	SGTYQRFG	AJ13
	1/12	CA	VSIG	NNRIFFG	AJ31
	1/12	CAA	RD	YGSSGNKLIFG	AJ32
	1/12	CA	VSR	DSNYQLIWG	AJ33
	1/12	CAAS	MK	GNTRKLIFG	AJ37
	1/12	C	TVTH	NNAGAKLTSG	AJ39
	1/12	CA	VS	NTEGADRLTFG	AJ45
	1/12	CAAS	L	ASSSFSKLVFG	AJ50
	1/12	CA	VSM	TGANTGKLTFG	AJ52
	1/12	CAA	FH	QGGSAKLIFG	AJ57

Brain	Clonal frequency	V	N	J	J gene	
Day 7						
#1	2/14	CAV	GTRA	QVVGQLTFG	AJ05	
	2/14	CAVS	MG	NSGTYQRFG	AJ13	¶
	2/14	CA	VSAA	SSGQKLVFG	AJ16	
	2/14	CAV	LMS	TGSNRLTFG	AJ28	
	1/14	CAVS	KG	NSGTYQRFG	AJ13	⊖
	1/14	CAVS	ADG	QGGRALIFG	AJ15	
	1/14	CAV	HI	DRGSALGRLHFG	AJ18	
	1/14	CAV	AGG	TNTGKLTFG	AJ27	
	1/14	CAV	PA	FASALTFG	AJ35	
	1/14	CAVS	PA	VGDNSKLIWG	AJ38	
#2	2/12	CAVS	M	TNSAGNKLTFG	AJ17	
	2/12	CA	ATT	ASLGKLQFG	AJ24	
	2/12	CAAS	PP	NNYAQG	AJ26	
	1/12	CA	SALN	NTGYQNFYFG	AJ49	
	1/12	CAVS	MG	NSGTYQRFG	AJ13	¶
	1/12	CAVS	IG	NSGTYQRFG	AJ13	§
	1/12	CAVS	VG	NSGTYQRFG	AJ13	
	1/12	CAVS		SNTNKVVFG	AJ34	
	1/12	CA	VL	SSSFSKLVFG	AJ50	
#3	2/13	CAVS	RG	NSGTYQRFG	AJ13	
	2/13	CAV	M	RGSALGRLHFG	AJ18	
	2/13	CA	ASEA	GFASALTFG	AJ35	
	2/13	CAAS	GAS	GGSNAKLTFG	AJ42	
	1/13	CAVS	KG	NSGTYQRFG	AJ13	⊖
	1/13	CA	ASPL	TNTGKLTFG	AJ27	
	1/13	CA	SLL	NTNKVVFG	AJ34	
	1/13	CAVS	TNT	NVGDNSKLIWG	AJ38	
	1/13	CA	SGM	GADRLTFG	AJ45	

FIGURE 4. *A*, Increase in the percentage frequencies of T cells bearing VA1-1, VA2-1, VB5-2, and VB8-2 in WNV-infected mouse brains. *B*, Amino acid sequences of CDR3 regions of VA1-1 in WNV-infected mouse brains on day 4 and day 7 postinfection. Identical sequences detected in different individual mice are marked by the symbols.

A

VA 1-1

Brain	Clonal frequency	V	N	J	J gene	
#1	24/51	CAVS	IG	NSGTYQRFG	AJ13	§
	21/51	CAVS	MG	NSGTYQRFG	AJ13	¶
	3/51	CA	ASGL	SNTNKVVFG	AJ34	
	2/51	CAVS	KG	NSGTYQRFG	AJ13	Θ
	1/51	CA	AL	NTGYQNFYFG	AJ49	
#2	33/52	CAVS	LA	NSGTYQRFG	AJ13	
	8/52	CAVS	RG	NSGTYQRFG	AJ13	
	6/52	CAVS	MG	NSGTYQRFG	AJ13	¶
	3/52	CAVS	MG	GYQNFYFG	AJ49	†
	1/52	CA	ASME	GDNSKLIWG	AJ38	
	1/52	CA	AED	YANKMICG	AJ47	
#3	13/50	CAVS	PG	NSGTYQRFG	AJ13	‡
	9/50	CA	AN	NVGDNSKLIWG	AJ38	⁎
	8/50	CA	ASM	TGNTRKLIFG	AJ37	
	6/50	C	GGKEG	GADRLTFG	AJ45	
	4/50	CAVS	MG	NSGTYQRFG	AJ13	¶
	3/50	CAVS	MG	GYQNFYFG	AJ49	†
	3/50	CAVS	PA	NSGTYQRFG	AJ13	
	2/50	CAV		NTNTGKLTFG	AJ27	
	1/50	C	GGKG	GSALGRLHFG	AJ18	
	1/50	CA	AS1	NTNTGKLTFG	AJ27	
#4	26/52	CAV	RPT	ASLGKLQFG	AJ24	
	15/52	CAVS	IG	NSGTYQRFG	AJ13	§
	6/52	CAVS	RG	QGGRALIFG	AJ15	
	3/52	CAAS	P	SGGSNAKLTFG	AJ42	
	2/52	CA	ASEMD	YANKMICG	AJ47	
#5	18/51	CAVS	KG	NSGTYQRFG	AJ13	Θ
	12/51	CAVS		TNAYKVIFG	AJ30	
	9/51	CAVS	R	TQVVGQLTFG	AJ05	
	7/51	CAVS	PG	NSGTYQRFG	AJ13	‡
	4/51	CA	AN	NVGDNSKLIWG	AJ38	⁎
	1/51	CAV	LTG	GADRLTFG	AJ45	

B

VA 2-1

Brain	Clonal frequency	V	N	J	J gene	
#1	34/50	CAAS	EG	GNYKYVFG	AJ40	§
	6/50	CA	PRG	NNYAQGLTFG	AJ26	
	5/50	CAAS	EG	TNTGKLTFG	AJ27	
	3/50	CAA	VD	YANKMICGLG	AJ47	
	2/50	CAA		TGGNNKLTFG	AJ56	
#2	18/53	CAAS	G	GSALGRLHFG	AJ18	
	15/53	CAAS	VA	GNYKYVFG	AJ40	
	14/53	CAAS	EA	GNYKYVFG	AJ40	¶
	3/53	CAA	NEA	GNYKYVFG	AJ40	
	2/53	CAAS	AVY	NTNTGKLTFG	AJ27	
	1/53	CAAS	VS	SGGNYKPTFG	AJ06	
#3	15/52	CAA	RG	NNYAQGLTFG	AJ26	
	11/52	CAAS	EA	GNYKYVFG	AJ40	¶
	7/52	CAAS	G	NNYAQGLTFG	AJ26	
	6/52	CA	VRG	NNYAQGLTFG	AJ26	
	6/52	CAAS	EG	GNYKYVFG	AJ40	§
	5/52	CAAS	ET	GNYKYVFG	AJ40	
	2/52	CAA	RD	VGDNSKLIWG	AJ38	
#4	21/52	CAAS	EA	GNYKYVFG	AJ40	¶
	14/52	CAAS	P	TNAYKVIFG	AJ30	
	12/52	CAA	I	TGGNNKLTFG	AJ56	
	4/52	CAAS	MA	GNYKYVFG	AJ40	
	1/52	CA	G	NNNAGAKLTFG	AJ39	
#5	17/50	CAAS	EA	GNYKYVFG	AJ40	¶
	11/50	CAAS	LA	GNYKYVFG	AJ40	
	9/50	CAA	RGN	YAQGLTFG	AJ26	
	8/50	CAAS	NA	NAYKVIFG	AJ30	
	3/50	CAAS	AGD	NYAQGLTFG	AJ26	
	2/50	CA	V	NAGAKLTFG	AJ39	

C

VB 5-2

Brain	Clonal frequency	V	N-D-N	J	J gene
#1	49/52	CASS	PGTGG	YEQYFG	BJ2. 7
	3/52	CASS	RTG	SAETLYFG	BJ2. 3
#2	46/53	CASS	RGD	YAEQFFG	BJ2. 1
	5/53	CAS	FRGD	YAEQFFG	BJ2. 1
	2/53	CASS	GTGG	NERFFG	BJ1. 4
#3	34/51	CASS	LEL	YAEQFFG	BJ2. 1
	13/51	CASS	PEL	YAEQFFG	BJ2. 1
	4/51	CASS	LDP	EQYFG	BJ2. 7
#4	26/51	CASS	PRD	NYAEQFFG	BJ2. 1
	15/51	CASS	LGGG	SYEQYFG	BJ2. 7
	8/51	CASS	LLDN	AETLYFG	BJ2. 3
	2/51	CASS	LTGA	NTEVFFG	BJ1. 1
#5	42/51	CASS	LRDS	YAEQFFG	BJ2. 1
	9/51	CASS	LNRV	YAEQFFG	BJ2. 1

D

VB 8-2

Brain	Clonal frequency	V	N	J	J gene
#1	18/52	CASG	DWGGAQ	SQNTLYFG	BJ2. 4
	10/52	CASG	DRTGL	NERLFFG	BJ1. 4
	9/52	CASG	DWTGK	SQNTLYFG	BJ2. 4
	7/52	CASG	EWGG	AEQFFG	BJ2. 1
	3/52	CASG	DVGQG	NTEVFFG	BJ1. 1
	3/52	CAS	SATTGG	NSDYTFG	BJ1. 2
	2/52	CASG	DDR	YEQYFG	BJ2. 7
#2	28/53	CASG	DWAGFS	SYEQYFG	BJ2. 7
	9/53	CAS	SDDRG	SAETLYFG	BJ2. 3
	9/53	CASG	DPGG	SYEQYFG	BJ2. 7
	3/53	CASG	ESGARD	NSPLYFA	BJ1. 6
	2/53	CAS	SPGTP	SYEQYFG	BJ2. 7
	1/53	CAS	SDGTGDN	NSPLYFA	BJ1. 6
	1/53	CASG	ERAGFS	SYEQYFG	BJ2. 7
#3	16/50	CASG	DWG	DTQYFG	BJ2. 5
	13/50	CASG	DAG	NQDTQYFG	BJ2. 5
	8/50	CASG	DAWGR	EQYFG	BJ2. 7
	7/50	CASG	DWTGDT	YAEQFFG	BJ2. 1
	3/50	CASG	DGGG	EQYFG	BJ2. 7
	2/50	CASG	DWTGGAG	QNTLYFG	BJ2. 4
	1/50	CASG	DWTGD	NYAEQFFG	BJ2. 1
#4	32/51	CASG	GLGS	SAETLYFG	BJ2. 3
	8/51	CASG	DWTGGD	ERLFFG	BJ1. 4
	5/51	CASG	DAGN	SYEQYFG	BJ2. 7
	4/51	CASG	DWTGGALG	QNTLYFG	BJ2. 4
	2/51	CASG	DL	YNSPLYFAAG	BJ1. 6
#5	16/50	CASG	GTGGL	NTLYFG	BJ2. 4
	13/50	CASG	EPGGA	NTLYFG	BJ2. 4
	8/50	CASG	DARD	SNERFFG	BJ1. 4
	4/50	CAS	RPRDWGN	YEQYFG	BJ2. 7
	3/50	CASG	DARTN	SGNTLYFG	BJ1. 3
	3/50	CAS	SDWGA	SAETLYFG	BJ2. 3
	2/50	CASG	AQGG	ETLYFG	BJ2. 3
	1/50	CASG	DEE	NTLYFG	BJ2. 4

FIGURE 5. Amino acid sequences of CDR3 regions of VA1-1 (*A*), VA2-1 (*B*), VB5-2 (*C*), and VB8-2 (*D*) in WNV-infected mice brain on day 10. In each family, identical sequences detected in different individual mice are marked by the symbols.

YVFG and CAAS-EA-GNYKYVFG) appeared from the brains of different mice. These clonotypes had similar CDR3 sequences and the common AJ40 segment. Sequence analysis with VB5-2 exhibited extremely high levels of oligoclonality: 49 of 52 clones in mouse 1, 46 of 53 clones in mouse 2, 34 of 51 clones in mouse 3, 26 of 51 clones in mouse 4, and 42 of 51 clones in mouse 5 had identical CDR3 sequences (Fig. 5*C*). However, these dominant VB5-2 clonotypes were different among the brains of mice. Similarly, dominant clonotypes obtained from VB8-2 had different CDR3 sequences among individual mice (Fig. 5*D*). These results indicated that oligoclonal T cells expanded in the brains of mice in response to WNV infection, and that the brain-infiltrating T cells used a highly restricted and shared TCRAV repertoire, but a somewhat diverse TCRBV repertoire.

To clarify T cell clonalities at an early time point during infection, we performed CDR3 sequence analyses using samples obtained from the brains on days 4 and 7 (Fig. 4). Brain T cells showed a more diverse TCR repertoire on days 4 and 7 compared with those on day 10 (Fig. 4*B*). On day 7, T cells showed some degree of oligclonality, and interestingly, several clonotypes (CAVS-MG-NSGTYQRFG, CAVS-KG-NSGTYQRFG, and CAVS-IG-NSGTYQRFG) that presented dominantly on day 10 were obtained at low frequency on day 7 (Fig. 4*B*). These results suggest that oligoclonal T cells are generated by local expansion within the brains, not migration from the periphery.

Comparison of the TCR repertoire among closely related flaviviruses

TCR repertoires were also analyzed with spleens and brains from mice infected with closely related flaviviruses, JEV and TBEV (Fig. 6). The percentage frequencies of T cells bearing VA1-1, VA3-1, and VB9-1 were significantly higher in the brains of TBEV-infected mice than in the spleens from mock-infected mice. We have previously reported that the percentage frequencies of T cells bearing VA5-1, VA17-1, VA19-1, VB2-1, VB8-3, and VB13-1 were significantly increased in the brains of JEV-infected mice (7). These results demonstrated that TCR repertoires used by the brain-infiltrating T lymphocytes were different among WNV-,